Stirling Engines

Ramla Gheith, Houda Hachem, Fethi Aloui, Sassi Ben Nasrallah

Stirling Engines

Ramla Gheith and Houda Hachem, University of Monastir, Monastir, Tunisia
Fethi Aloui, University of Valenciennes (UVHC), Valenciennes, France
Sassi Ben Nasrallah, University of Monastir, Monastir, Tunisia

Nomenclature

A	Fluid passage section through heat exchanger (m^2)
C_p	Heat capacity of the cooling water (J kg^{-1} K^{-1})
d_{hyd}	Hydraulic diameter (m)
d	Diameter (m)
dt	Cycle time (s)
$\delta\dot{Q}_{Cdr}$	Internal conduction loss in regenerator (W)
$\delta\dot{Q}_{vr}$	Viscous friction loss in regenerator (W)
Δp	Pressure drop (bar)
ΔT	Temperature difference between inlet and outlet cooling water (K)
η_{el}	Electric efficiency (%)
η_m	Mechanical efficiency (%)
η_{th}	Thermodynamic efficiency (%)
ε	Efficiency (%)
f	Darcy friction factor throw a porous medium
f	Frequency (Hz)
f_r	Friction factor through a porous medium
h	Height (m)
K	Permeability of a porous medium (m^2)
μ	Dynamic viscosity of the working fluid (Pa. s)
$\dot{m}_w$	Mass flow of the cooling water (kg s^{-1})
$\dot{m}$	Mass flow rate through the heat exchanger (kg s^{-1})
N	Rotational speed (rpm)
NUT	Number of transfer units
Nu	Nusselt number
NUTr	Number of transfer units of regenerator
Nk	Effective gas conductivity due to thermal dispersion related to of molecular conductivity
P	Pressure (bar)
ϕ	Porosity
Pr	Prandtl number
Q	Flow rate (m^3 s^{-1})
$\dot{Q}_{irr}$	Effective thermal power exchanged in regenerator(W)
Q_L	Removed heat from the cold reservoir (J)
Q_H	Supplied heat to the hot reservoir (J)
Re	Reynolds number
ρ	Density (kg m^{-3})
ρ_m	Density of matrix solid material (kg m^{-3})
T	Temperature (K)
T_0	Temperature reference which is equal to ambient temperature (K)
T_H	Temperature of the high-temperature reservoir (K)
T_L	Absolute temperature of the low-temperature reservoir (K)
u	Axial velocity (m s^{-1})
V	Volume of the heat exchanger (m^3)

Indices

g	Working gas
h	Heater
hyd	Hydraulic
k	Cooler
k-r1	Interface between cooler and regenerator
r	Regenerator
m	Regenerator constituting material
r2-h	Interface between regenerator and heater
r1-r2	Interface between first and second section of the regenerator
wh	Heater wall temperature
wk	Cooler wall temperature

4.6.1 Introduction

The industrial revolution in the 19th century led to both a great necessity to produce thermal energy and several environmental accidents. After the oil booms and the increase of oil price many industries closed and the industrial areas become brownfields (polluted areas that cannot be used for housing or for agriculture). All these events led to an increase in awareness about

environmental problems. Also, governments became more involved in climate change problems. Hence the resumption of interest in alternative solutions.

The Stirling engines were invented in 1816, by Robert Stirling (see Relevant Websites section). The regenerator is considered as an added value of Stirling engine performances but they are the seat of an important part of thermal losses recorded in such engines.

The regenerator is a porous medium used to economize heat for/from the working fluid [1,2]. All the exchanged heat energy passes through it and is proportional to its performances [3]. A Stirling engine without a regenerator needs five times more energy to produce the same performances as an engine including a regenerator [4]. According to Gheith *et al.* [3], a performant regenerator needs to have high thermal capacity [5] and conductivity [6], large surface area [7], small dead volume with dense matrix [8,9], and highly porous matrix with minimum resistance to flow [10].

Several studies treated numerically the heat exchange, the design, and the losses inside Stirling engine regenerator [10–13], but few experiments have been made. Stirling engine regenerators are very complex to model and design. It will require a large number of equations to describe their thermodynamic behavior (material side and working fluid side). The engine performances are more sensitive to a change in the regenerator efficiency and its ability to accommodate the high heat flow. The regenerator efficiency increase leads to an increase of the exchanged thermal energy through it and consequently an amelioration of engine brake power [14]. Tlili *et al.* [15] showed that the energy lost in the regenerator represents 86% of the total energy lost in the engine. Hachem *et al.* [14] showed that the regenerator is the set of 44% of viscous loss, 33% of internal conduction loss, and 22% of imperfection loss respectively from the total losses inside a Stirling engine. The determination of adequate material for Stirling engine regenerator is widely studied. Several materials have been used as Stirling regenerator [15–17], new material tested [18], and parameters influence detected [19–23].

4.6.2 Background and Fundamentals

4.6.2.1 Invention

In the 19th century, the industrial revolution needs a great thermal energy production. The used technologies (especially steam boilers) have several technical problems causing harm to humans and damaging materials. A safe external combustion engine was the invention proposed by Robert Stirling to save human life and materials [24]. The initial installation is represented in **Fig. 1**. Robert Stirling proposed quickly an amelioration of his installation by adding an economizer, which enhances the heat exchange inside the installation [25,26].

4.6.2.2 Evolution

Initially, in 1816, the Stirling engine was used to pump water from a stone quarry. In 1820, James Stirling (Robert's younger brother) introduced the working fluid at a pressure higher than atmospheric pressure in order to increase the output power of the engine. Until 1922, more than 25,000 Stirling engines were used either to pump water or to train electrical generators (see Relevant Websites section).

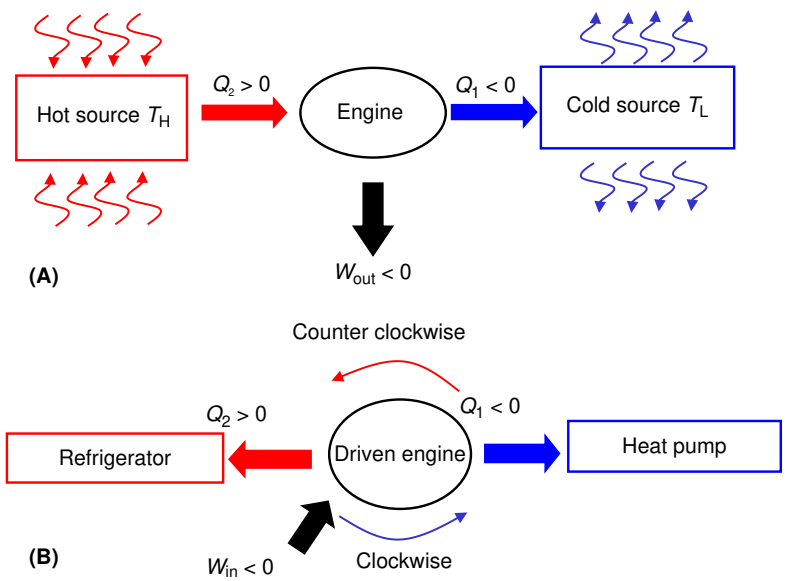

Fig. 1 Schematic view of Stirling machine working principle. (A) Hot air engine and (B) receiving machine.

Table 1 Maximum brake efficiencies for various Stirling engines

Engine designation	*Prototype*	*4-235 Prototype*	*40 HP Prototype*	*Anal. Ph. I Prototype*	*4-400 Prototype*
Manufacturer	United Stirling	Philips	Philips	United Stirling	MAN technology
Working fluid	H_2	He	H_2	H_2	He
Mean pressure (MPa)	14.5	22.1	14.2	14.5	10.8
Heater temperature (°C)	691	683	649	719	633
Cooler temperature (°C)	71	43	16	71	41
Power (kW)	35	175	23	76	88
Rotational speed (rpm)	2000	1800	725	1200	1000
Thermodynamic efficiency (%)	30	31	38	35	32
Carnot efficiency (%)	47	46	55	54	49
Engine type	2 pistons	Piston-Displacer	Piston-Displacer	2 pistons	Piston-Displacer
Number of cylinder	4	4	4	8	4

4.6.2.2.1 1936 – the Philips Stirling engine

The N. V. Philips Society of The Netherlands was the first great society interested in Stirling engine [27,28]. **Table 1** below recapitulates geometric and functioning characteristics, power and efficiency of same engine realized by Philips society.

The Philips society designed and manufactured a Stirling engine generator of radio. These radios can be used in isolation habitation, which is not connected to the public electricity network.

Philips Electronics Group developed a Stirling engine to power portable radios. These radios were designed for use in remote areas without access to electricity.

4.6.2.2.2 The Philips 1-98 engine

Only 30 engines of this type were manufactured. The 1-98 engine includes three heat exchangers, a single power piston and displacer, and a Rhombic drive system. The major problem of this installation was its heat exchangers. A second version of the installation was proposed with ameliorated heat exchanger.

4.6.2.2.3 From 1945 to 1975: Sleeping technology

During this period, the Stirling engine lost its competitiveness compared to systems with the same power. It was used in some military applications including ships and submarines.

4.6.2.2.4 1962 – Free piston engine

William Beale invented the free piston Stirling engine, which has no mechanical losses compared to classical installation.

4.6.2.2.5 Since 1975 – The rebirth

Given the energy and environmental problems many companies from various sectors such as automotive, marine propulsion, or heating systems are rediscovering technology somewhat forgotten and adapting it to their own process. New Stirling installations are patterned and commercialized such as microgen installation (see Relevant Websites section), Stirling dish, etc.

4.6.2.3 Stirling Cycle & Thermodynamic Assessment

4.6.2.3.1 Stirling cycle

The Stirling engine has the ability to work either in receiving mode or in driven mode (**Fig. 1**). The reversibility of the Stirling engine is an additional advantage. It can operate either in driven machine (produced work) or on receiving machine (heat transfer). The hot source can be from renewable energy (solar, recovered heat, biomass, etc.) and the cold source can be ambient air, water, or frigorific fluid (see Relevant Websites section).

The Stirling engine is working in a closed cycle (**Fig. 2**). The working fluid trapped inside the engine can be air, helium, CO_2, nitrogen, hydrogen, etc. It takes periodically four transformations, representing the Stirling cycle.

1. Isothermal compression process: the compression piston compresses the working fluid, so, the pressure increases. The temperature is maintained constant because of the heat flow from cooler to surroundings.
2. Isochoric regeneration (heat addition): the working fluid is transferred from compression space to expansion space through porous media regenerator. The working fluid is preheated in the regenerator.
3. Isothermal expansion: the expansion piston moves away from the regenerator. The pressure decreases as the volume increases. The temperature remains constant by adding heat to the system from the heater.
4. Isochoric regeneration (heat removal): both pistons move simultaneously to transfer working fluid from expansion space to compression space through regenerator at constant volume. The heat is transferred from the working fluid to the regenerator matrix.

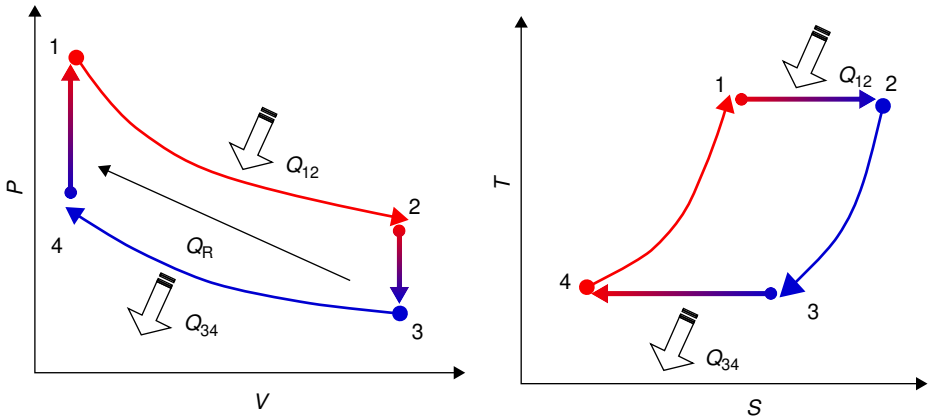

Fig. 2 Clapeyron diagram (*P*–*V*) and entropic diagram (*T*–*S*).

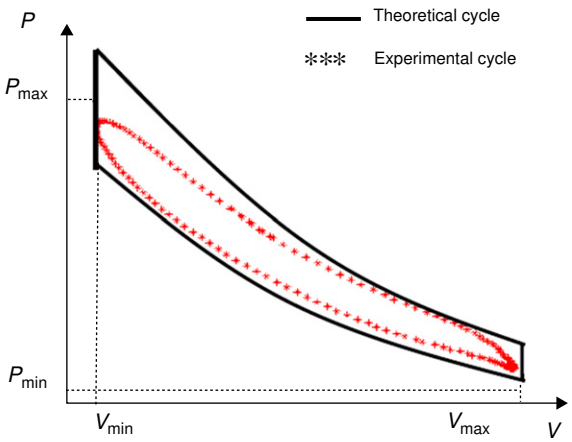

Fig. 3 Theoretical and experimental *P*–*V* diagrams.

The Stirling cycle has same advantage over the Carnot cycle [29,30]: (1) The replacement of two isentropic and two isochoric transformations, which increases the area of the *P*-*V* diagram. (2) Heating and cooling processes, which are improved by a regenerative porous media (see Relevant Websites section).

The experimental Stirling cycle is different from the theoretical one (**Fig. 3**) [31]. An important difference between both cycles (experimental and theoretical) can be noted. These differences are essentially explained by:

- Losses by friction and by singular pressure drop when the working fluid goes through heat exchangers.
- The real movements of the pistons are different from the theoretical movements.
- The great heterogeneity of the instantaneous temperatures in the thermal machine and to the irreversibility presents in the Stirling machine [32].
- The regenerator cannot follow the temperatures variations from the hot side to the cold one, and vice-versa. Indeed, the temperature of the regenerator reaches that of the hot source and does not fall anymore because of its big thermal inertia.
- The loss of the pressure drops recorded in the regenerator is important. It is due to its geometric aspects (weak diameter) and to its physical characteristic (weak porosity).

Hachem *et al.* [31] studied a Beta Stirling engine working in receiving mode. Knowing the volumes and the pressure evolutions they represented the PV diagrams of the refrigerator (**Fig. 4**) modes. The network transmitted to the machine is about 3.513 J at 126 rpm of rotational speed. Stirling heat pump has COP ranging from 2 to 3.4, implying that they deliver 2 to 3.4 times more energy than it consumes. The best COP is obtained at the less rotational speed inputted in the machine (103 rpm), the heat has an energetic COP of about 3.4 and an exergetic COP of 0.75.

4.6.2.3.2 Thermodynamic assessment

1. Engine mode
   The working fluid (the thermodynamic system) provides output work $\delta W < 0$. So, an amount of heat is added to the cycle by an external heat source and assigned to the cold source [33–35].

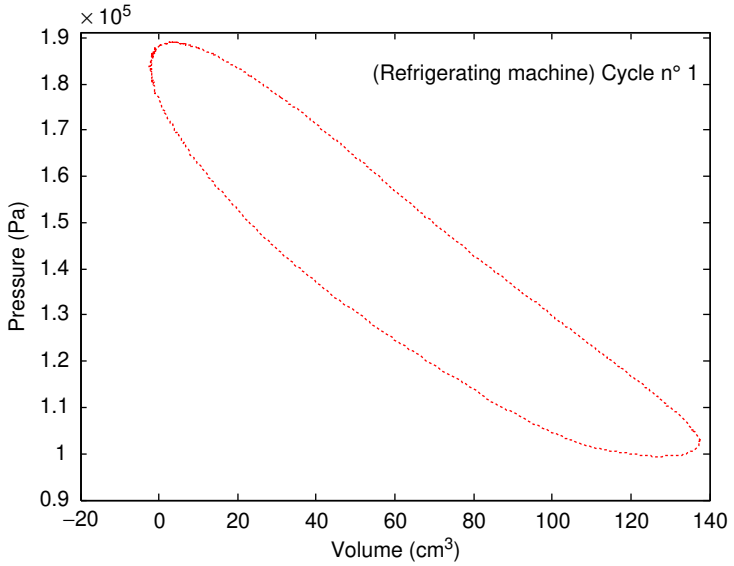

Fig. 4 *P–V* diagram at 126 rpm (refrigerating mode).

The theoretical thermal efficiency η_{th} of the Stirling engine is defined by:

$$\eta_{th} = \frac{\text{Produced work}}{\text{amount of heat received by the working fluid}} = \frac{-\delta W}{\delta Q} \tag{1}$$

In practice, due to the various heat losses (imperfect insulation, radiation, etc.), an addition among of heat $\delta Q'$ is dissipated by the engine. With consideration of these losses the thermodynamic efficiency can be formulated as:

$$\eta'_{th} = \frac{\text{amount of heat received by the working fluid}}{\text{amount of heat gived to the working fluid}} = \frac{-\delta Q}{\delta Q'} \tag{2}$$

Similarly, knowing the mechanical losses (especially mechanical friction), the mechanical work $\delta W'$ effectively recovered is less than δW, the mechanical efficiency (or organic) can be defined as:

$$\eta_{mec} = \frac{\text{Produced work}}{\text{indicated work}} = \frac{-\delta W'}{\delta W} \tag{3}$$

Consequently, a Stirling engine global efficiency can be estimated as follows:

$$\eta_{gol} = \frac{\text{Produced work}}{\text{dissipates amount of heat}} = \frac{-\delta W'}{\delta Q'} = -\frac{\delta W'}{\delta W} \times \frac{\delta W}{\delta Q} \times \frac{\delta Q}{\delta Q'} = \eta_{mec} \cdot \eta_{th} \cdot \eta_{cal} \tag{4}$$

Thermodynamic imperfections can be quantified as exergy destructions, which represent losses in energy quality or usefulness [31]. The exergy efficiency is presented to judge the ideality of a system. The exergy efficiency, also called the second law efficiency, is defined as the ratio of the actual thermal efficiency to the maximum possible (reversible) thermal efficiency under the same conditions:

$$\eta_{Ex} = \frac{\eta_{th}}{\eta_c} \tag{5}$$

It can also be expressed as the ratio of the exergy recovered (as useful input) and the exergy supplied (as total input):

$$\eta_{Ex} = \frac{\text{Energy recovered}}{\text{Energy supplied}} = 1 - \frac{\text{Energy destroyed}}{\text{Energy supplied}} \tag{6}$$

For a heat engine, the exergy supplied is the decrease in the exergy of the heat transferred to the engine, which is the difference between the exergy of the heat supplied and the exergy of the heat rejected. The network output is the recovered exergy. Finally,

the exergy efficiency is calculated as follows:

$$\eta_{Ex} = \frac{W_{out}}{Ex_{Q_H}} \tag{7}$$

The exergy efficiency η_{Ex} frequently gives a finer understanding of performance than the energy efficiency η_{th}. In evaluating efficiency, the same weight is assigned to energy whether it is shaft work or a stream of low-temperature fluid. The parameter η_{Ex} points out that there is a need to deal with all external and internal irreversibilities to improve the machine performance [31]. Finally, the overall efficiency of the Stirling heat engine is calculated as follows:

$$\eta_g = \frac{\text{Output work}}{\text{Electric energy supplied}} = \frac{-W}{Q_{in}} = -\frac{W}{Q_H}.\frac{Q_H}{Q_{in}} = \eta_{th}.\eta_{cal} \tag{8}$$

where η_{cal} is the calorific efficiencies of the hot heat exchanger (HEX).

2. Refrigerator mode

When an external work is applied to a Stirling engine, this latter will work a refrigerator. It can provide very low temperature. The coefficient of performance (COP) of the refrigerator can be estimated as follows:

$$COP_R = \frac{\text{Desired output}}{\text{Required input}} = \frac{|Q_L|}{W_{in}} = \frac{|Q_L|}{Q_H - Q_L} = \frac{1}{|Q_H/Q_L| - 1} \tag{9}$$

The amount of heat received from the low-temperature reservoir Q_L during one cycle is defined as the sum of the inputted work and the amount of heat rejected to the high-temperature:

$$Q_L = W_{in} + Q_H \tag{10}$$

The amount of heat rejected to the high-temperature reservoir Q_H during one cycle is calculated as follows:

$$Q_H = \dot{m}_w C_p \Delta T dt \tag{11}$$

The input work W_{in} is described as follows:

$$W_{in} = \frac{W_{el}}{\eta_{el}\eta_m\eta_{th}} \tag{12}$$

Additionally, the Carnot COP of a refrigerating cycle is defined as follows:

$$(COP)_C = \left(\frac{Q_L}{Q_H - Q_L}\right)_C = \frac{T_L}{(T_H - T_L)} \tag{13}$$

The COP_c is always greater than the COP of an irreversible refrigeration cycle when each operates at the same conditions. The thermal exergy for the refrigeration mode is defined as follows:

$$Ex_{QR} = \left(1 - \frac{T_0}{T_L}\right)|Q_L| \tag{14}$$

The exergetic coefficient of performance COP_{Ex} is calculated as follows:

$$COP_{ExR} = \frac{Ex_{QR}}{W_{in}} \tag{15}$$

Referring to the exergy balance:

$$\sum Ex_{in} = \sum Ex_{out} + \sum Ex^D \tag{16}$$

Thus, the amount of exergy destruction Ex^D in the Stirling refrigerator can be estimated as follows:

$$Ex_{QR}^D = W_{in} - Ex_{QR} \tag{17}$$

The exergy coefficient of performance COP_{Ex} frequently gives a finer understanding of performance than the energy COP. In evaluating COP, the same weight is assigned to energy whether it is shaft work or a stream of low-temperature fluid. The parameter COP_{Ex} points out that both external and internal irreversibilities need to be dealt with to improve the machine performance [36].

3. Heat pump mode

When an external work is provided to the Stirling engine and the flywheel is driven counterclockwise, the engine operates as a heat pump. The COP of the Stirling heat pump can be expressed as follows:

$$\mathrm{COP}_{\mathrm{HP}} = \frac{Q_{\mathrm{H}}}{W_{\mathrm{in}}} = \frac{Q_{\mathrm{H}}}{Q_{\mathrm{H}} - Q_{\mathrm{L}}} = \frac{1}{1 - (Q_{\mathrm{L}}/Q_{\mathrm{H}})} \tag{18}$$

The real heat pump COP is always less than the reversible Carnot efficiency given as follows:

$$(\mathrm{COP})_{\mathrm{C}} = \left(\frac{Q_{\mathrm{H}}}{Q_{\mathrm{H}} - Q_{\mathrm{L}}}\right)_{\mathrm{C}} = \frac{T_{\mathrm{H}}}{T_{\mathrm{H}} - T_{\mathrm{L}}} \tag{19}$$

The thermal exergy for heat pump mode is defined as follows:

$$\mathrm{Ex}_{Q_{\mathrm{HP}}} = \left(1 - \frac{T_0}{T_{\mathrm{H}}}\right) Q_{\mathrm{H}} \tag{20}$$

Then the exergy COP for heat pump can be calculated as:

$$\mathrm{COP}_{\mathrm{Ex}_{\mathrm{HP}}} = \frac{\mathrm{Ex}_{Q_{\mathrm{HP}}}}{W_{\mathrm{in}}} \tag{21}$$

Finally, energy and exergy formulations even for heat pump and refrigerating machine are applied to the experimental operating data obtained from the Beta Stirling machine.

4.6.2.4 Stirling Engine Classification

Since their invention by Robert Stirling, the Stirling engine has undergone several transformations. Three levels of categorization are generally used:

- the cylinder composition
- the cylinders arrangement
- the pistons coupling

In addition to these classifications, several particular Stirling engines are available.

4.6.2.4.1 Simple or double acting Stirling engine

The single-acting Stirling engines are constituted by a piston and a displacer, which can be included in the same cylinder or separated into two separate cylinders. The compression and expansion fields are in communication through a regenerator.

The double-acting engines are essentially constituted of two or more pistons. In these engines, each piston acts as a displacer for the piston in its vicinity. The great advantage of this kind of arrangement is that the number of pistons is halved, which significantly reduces the cost of such engine.

A schematization of the Stirling engine simple and double effect are presented in **Fig. 5**.

4.6.2.4.2 Mono or multiphasic Stirling engine

Mono or multiphase Stirling engines classification is obtained according to the thermodynamic state of the fluid, which may be two phases, for example, in the Fluidyne [37]. Fluidyne is the name given to a class of Stirling engines in which the pistons are actually columns of liquid (usually water) moving up and down in a set of U-tubes [37].

4.6.2.4.3 Resonant or not resonant

This distinction is only relevant for the free piston engines and Fluidyne. The resonant mode of operation corresponds to machines with a displacer and a piston moving continuously and, in most cases, sinusoidal. Or nonresonant mode ("over driven") corresponds to operation in which the movement of the displacer and/or the piston is discontinuous.

An ameliorated version of FSE was proposed by Boucher *et al.* [38]. They proposed a study of DFPSE working with helium. The DFPSE produces a mechanical power of 1 kW and it has a design operating point of 1.4 MPa corresponding to the frequency about 22 Hz.

4.6.2.4.4 Classification according to the cylinders arrangement

According to the kinematic arrangement of its different compartments, the Stirling engine can be classified in three major configurations: Alpha, Beta, and Gamma (**Fig. 6**). The Alpha configuration is the simplest building Stirling engine, characterized by its compactness. The Beta configuration is mainly composed of a simple piston placed coaxially with a displacer. This configuration presents serious sealing problems. The Gamma configuration is the oldest and the most cumbersome one. It is composed of two separate working spaces, which causes an important dead volume. This latter compromises the effective expansion temperature and hence the engine efficiency. The diversity of Stirling engine configurations is a constraint to their development and specifically to their standardization. However, this diversity has extended its applications to several areas: dish Stirling, wood boiler, electricity production, engine propulsion, etc. Three configurations can be mainly listed [11].

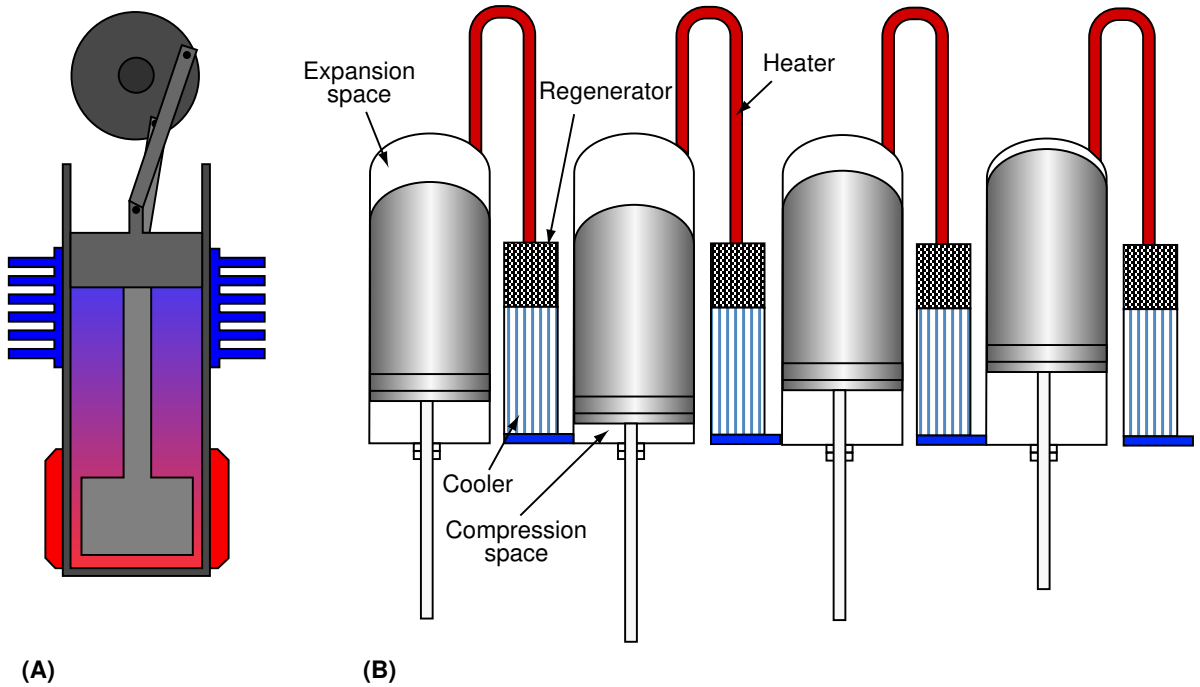

Fig. 5 Simple (A) and double (B) acting Stirling engine. Reproduced from Descombes G, Magnet JL. Moteur non conventionnels. Techniques de l'ingénieur, BM 2 593; 1997. p. 1–34.

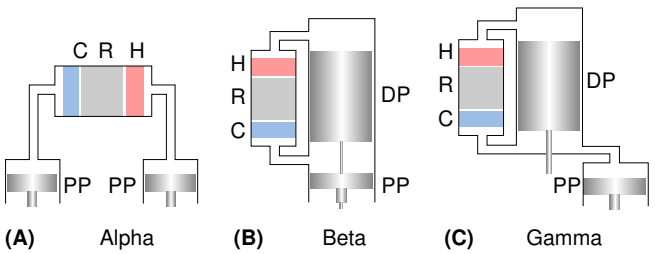

Fig. 6 The three main configurations of Stirling engines, such as: C, Cooler; DP, Displacer; H, Heater; PP, Power piston; R, Regenerator. Reproduced from Wang K, Sanders SR, Dubey S, Choo FK, Duan F. Stirling cycle engines for recovering low and moderate temperature heat: a review. Renew Sustain Energy Rev 2016;62:89–108.

The Beta engine [39,40] includes the set of Stirling engines with a single cylinder pact and where the displacer and the power piston are linked in tandem. It is the most complicated configuration. The power is generated by the action of the pistons jointly. This type of configuration has sealing problems but has the advantage of compactness, lower dead space involved, and overlapping of volume.

The Gamma engine [41] is very comparable to beta-group since the power output is generated in the same way as in Beta engines. The only difference is that the two pistons move in separate cylinders. This configuration has an important dead volume and produces a lower compression ratio, but it is usually simpler mechanically and is often used in multicylinder Stirling engines (**Figs. 7** and **8**).

4.6.2.4.5 Classification by pistons coupling

Three different types of pistons coupling are distinguished for Stirling engine:

- the rigid coupling (kinematic engines)
- the gas connection (free-piston engines)
- the fluid coupling

1. The rigid coupling (kinematic engines): engines' rigid coupling (or kinematic) uses a mechanical link between pistons. The main considerations for the choice of a coupling mechanism are the following:
   - Look for simple systems that are thus inexpensive in manufacture and maintenance.
   - Search systems allowing the highest possible seal, because one of the characteristics of the Stirling engine is operating at relatively high pressures.

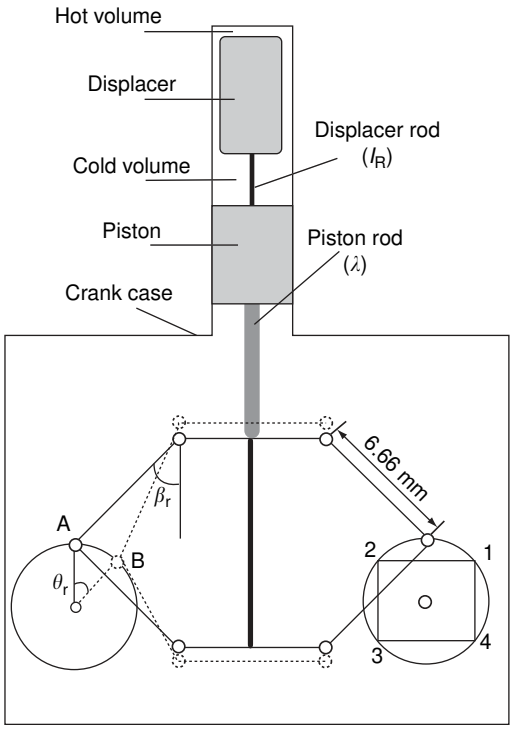

Fig. 7 Schematic illustration of the Rhombic driven Stirling engine.

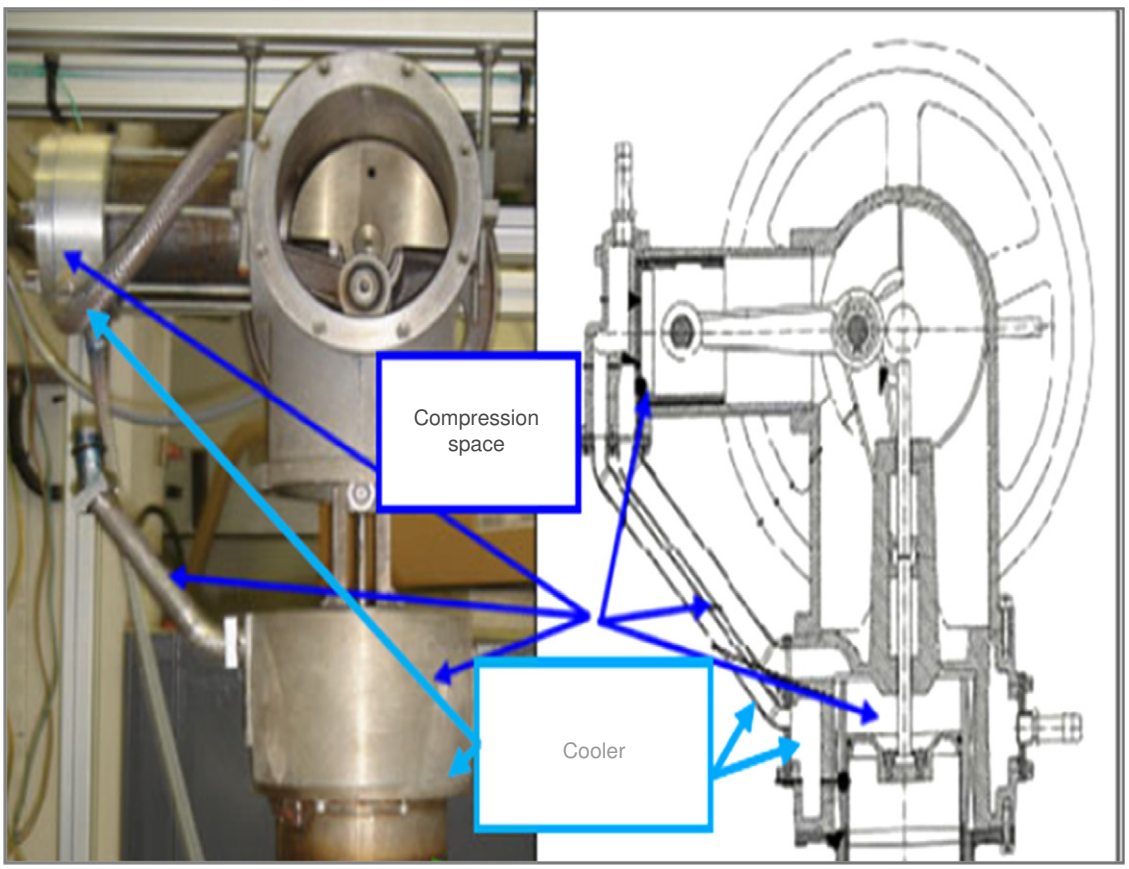

Fig. 8 Stirling engine with a crank and rod connection system. Reproduced from Gheith R, Aloui F, Tazerout M, Ben Nasrallah S. Experimental investigations of a Gamma Stirling engine. Energy Res 2012;36:1175–82.

2. Crank and rod system: the most commonly used mechanism is the drive crank device. It is often used for transmitting rotary motion from a reciprocation one and allows a 90 degree phase shift between the pistons. This type of mechanism is used for smaller engines but has the major disadvantage of not allowing the dynamic balancing of a single cylinder engine [42].

   Using the Ross yoke linkage (**Fig. 9**) is well known because of the high power-to-volume ratio. However, the thermodynamic analysis of this engine was so restricted according to a literature overview since it is reported to necessitate high temperature, but this problem was solved after the latest technological advances [42] (**Fig. 10**).

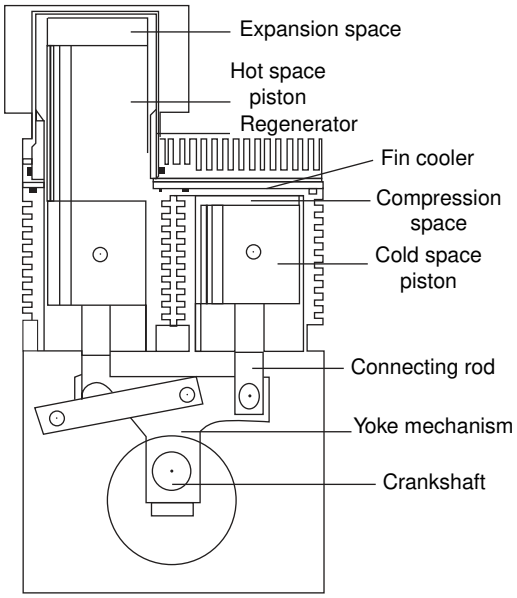

Fig. 9 The Yoke Ross driven mechanism. Reproduced from Tlili I, Musmar SA. Thermodynamic evaluation of a second order simulation for Yoke Ross Stirling engine. Energy Convers Manag 2013;68:149–60.

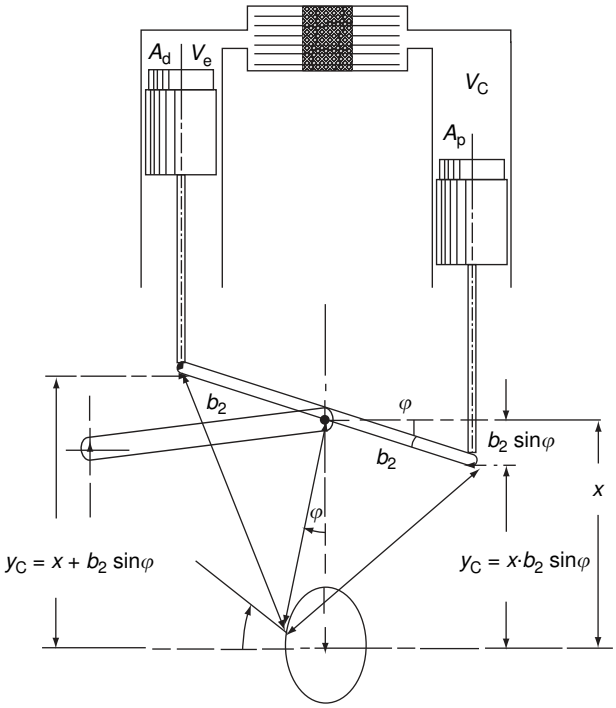

Fig. 10 Geometric derivation of the Yoke Ross drive. Reproduced from Tlili I, Musmar SA. Thermodynamic evaluation of a second order simulation for Yoke Ross Stirling engine. Energy Convers Manag 2013;68:149–60.

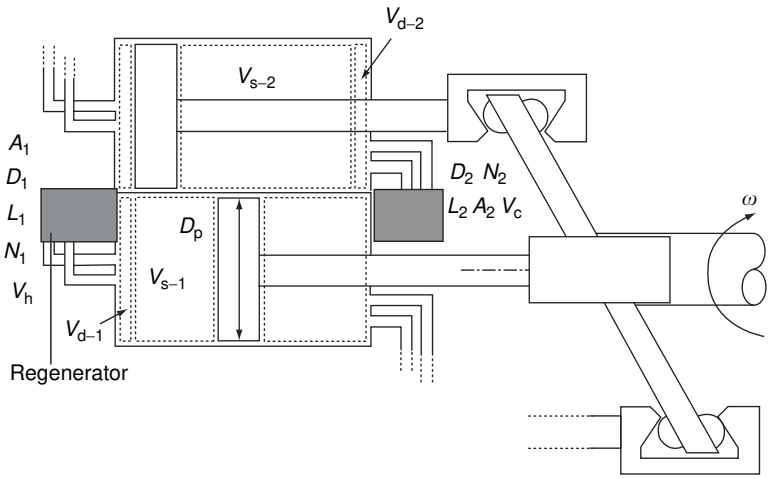

Fig.11 Schematic representation of the sliding disk mechanism ("swashplate"). Reproduced from Campos MC, Vargas JVC, Ordonez JC. Thermodynamic optimization of a Stirling engine. Energy 2012;44:902–10.

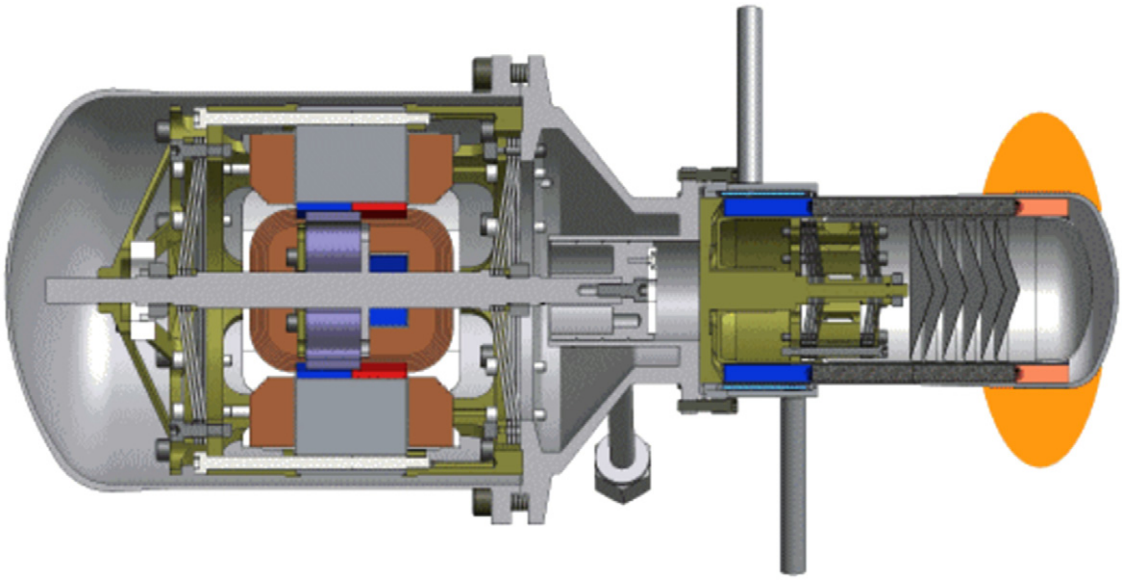

Fig. 12 Free piston Stirling engine.

3. The rhombic drive mechanism: the evolution of the Stirling engine for a wide range of power has led to isolate the cylinder crankcase and avoid pressurizing the entire crankcase. Rhombic command (**Fig. 7**) was developed by Philips for converting a linear motion into a rotary motion. This system must be designed and made with great care and good precision for satisfactory mechanical efficiency. It has the advantage of being dynamically balanced even for a single cylinder machine. The disadvantage of this movement is due to the large number of moving parts.
4. The splash plate: the "Swashplate" (**Fig. 11**) is a device used in mechanical engineering to translate the rotary motion of a shaft into a reciprocating, translating, or reciprocating motion to a rotating crankshaft to replace the engine to drawings. In this system each drive rod is connected to a rotating inclined plate, which generates the reciprocating movement of the pistons. The angle of inclination of the plate allows varying the stroke of the pistons and thus varying the power output. This system provides a good balance of the engine [43]. Meijer [44] proposed a method to control the engine performances by adjusting the swashplate angle.

4.6.2.4.6 Gas coupling (free-piston engines)

The free piston Stirling engine (**Fig. 12**) [45] has the particularity to convert the thermal energy in a directly usable energy. This configuration incorporates within a single, hermetically sealed transfer piston, while the free piston acts directly on the driven

engine. Its efficiency is greater compared to the kinematic engines because of the absence of driving mechanism (crankshaft, crank rod) [46].

Free-piston machines are therefore characterized by lower cost, longer service life and minimal maintenance compared to kinematic Stirling engines. The rapid movement of the displacement piston has the advantage of bringing the actual cycle of the motor of the theoretical cycle of Stirling into effect. There are different types of free-piston machines among which the Martini machine, the Ringbom machine, and the Stirling free-displacement (FPFD) machine (see Relevant Websites section).

4.6.2.4.7 Liquid coupling (Fluidyne)

For this Stirling engine class, the pistons are connected by means of a liquid. In most cases, the pistons are themselves liquids. An interesting example is the motor called "Fluidyne," which consists of oscillating liquid column [47].

It is a "pump-motor" based on the simple Stirling cycle. It is rustic, inexpensive, and easy to implement. The Fluidyne water pump is a machine for converting low-temperature thermal energy by bringing external heat (solar, rejects, etc.). Even if its thermal efficiency remains relatively low, this type of machine can be used as an inexpensive means of irrigation using an extremely simple technology with a minimum of moving parts [37].

4.6.2.5 Applications

4.6.2.5.1 Electricity production from solar energy

Many companies are trying to revive the Stirling engine as a source of electrical energy (see Relevant Websites section). Some industries have developed Stirling engines to exploit solar energy reflected by a parabolic collector (**Table 2**). Among these contributions we find the system infinea [52] or solar dish [53]. Other precommercial prototypes (see Relevant Websites section) have been developed in the field of cogeneration of electricity and heat (CHP), the cogeneration units Cleanenergy [51], Whispergen [54], Stirling DK, and the "Sunmachine" gas or biomass [55]. All solutions are based on high-temperature sources. In the field of low-temperature differences, it is proved experimentally that the Stirling engine can operate with only a few degrees of temperature difference. But all the experienced engines remain miniature models [56–58].

Actually, only about 10% of the world's electricity is generated by cogeneration. Exceptions are some European countries, such as Denmark and Finland, which have successfully expanded the use of cogeneration to 30%–50% of total electricity production in recent years [59]. Microcogeneration systems are reducing CO_2 emissions, reducing the need for electricity transmission and distribution networks, and making beneficial use of local energy resources (e.g., through the use of waste, biomass, solar energy, thermal heat releases, and others).

4.6.2.5.2 Electricity generation from biomass

Stirling engine installation can be used to generate electricity from biomass. This installation is mainly for domestic use since the installation is silent and safe (no risk to have vibrations due to explosion). The CHP "Stirling DK" cogeneration unit (**Fig. 13(A)**) is studied by Obernberger *et al.* [60], who have designated a heat exchanger for a Stirling engine coupled to a biomass boiler. The heat exchangers consist of a series of U-shaped tubes surrounding the combustion chamber to favorize convective and radiative transfer.

The CHP cogeneration unit of "Sunmachine" (**Fig. 13(B)**) is a wood pellet boiler that produces hot water and electricity for domestic use. It has an overall efficiency of about 90%, thermal power 4.5–10.5 kW and electrical power 1.5–3 kW. The Stirling wood boiler, shown in **Fig. 11(C)**, is already sold in a thousand copies in the Northern European countries. It is a boiler that heats a house with wood pellets and produces the electricity of the house. This model has a power of 15 kW thermal (hot water) and 1 kW electric. However, the problem of particles emerging from the combustion of wood remains.

4.6.2.5.3 Electricity generation from nuclear energy

NASA and other space agencies use the Stirling engine to provide electrical power to satellites and space probes in addition to solar panels, which it helps to orient to maximize efficiency. Currently, NASA is conducting studies regarding the installation of a permanent base on the moon. To generate electricity at this station, NASA is considering a small nuclear power plant that generates heat for a free-piston Stirling engine. The cold source would consist of large radiators. The Stirling engine must have a good efficiency and especially a very good power/mass ratio. This last point is crucial in the space domain to limit the mass of fuel embarked by the launching rocket.

Table 2 Performance and operating conditions of some Stirling engines used for thermoelectric conversion of solar energy

Stirling engine model	*Power (kW)*	*Efficiency (%)*	*Working gas*	*Displacement (cc)*	*Rotational speed (rpm)*	*Number of cylinders*	*Refs.*
Solo 161	10	–	He	160	1500	2	[48,49]
STM 4-120	25	–	H_2	480	2200	4	[50]
SES 4-95	25	Between 38% and 40%	H_2	380	1800	4	[51]

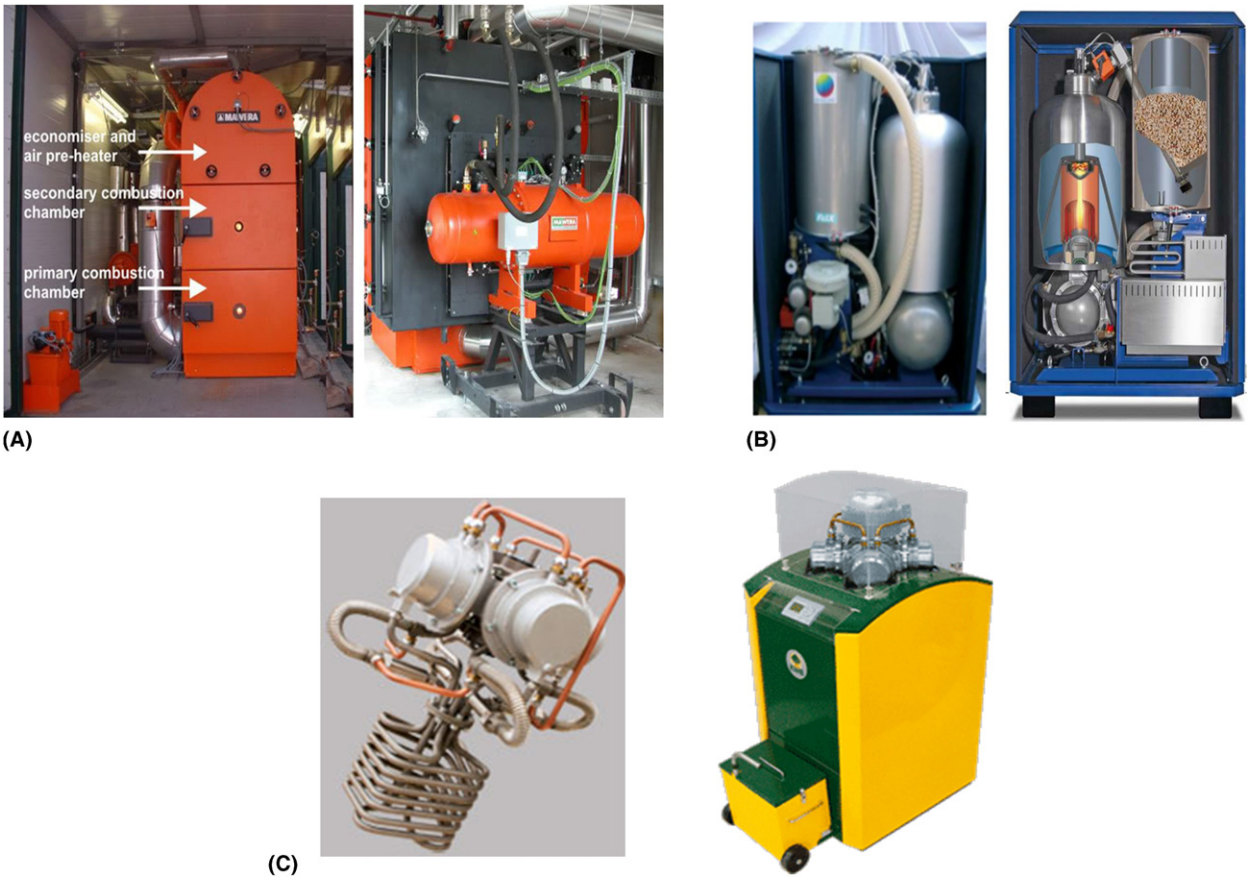

Fig. 13 Stirling engine cogeneration unit working with biomass. (A) Cogeneration unit "Stirling DK" ayant une puissance de 35 kW au Denmark (biomass, gasification) (Reproduced from Obernberger I, Carlsen H, Biedermann F. State-of-the art and future developments regarding small-scale biomass CHP systems with a special focus on ORC AND Stirling engine technologies. In: International Nordic bioenergy conference; 2003.). (B) Microcogeneration unit "Sunmachine" (biomass, pellets) (Reproduced from Crema L. *et al.*, Development of a pellet boiler with Stirling engine for m-CHP domestic application. Energy, Sustain Soc 2011;15.). (C) Wood Stirling micro CHP boiler (Reproduced from Stirlingpowermodule. Available from: www.stirlingpowermodule.com.).

4.6.2.5.4 Residual electricity generation from natural gas

According to De Paepe *et al.* [61], cogeneration systems are attractive for residential use. Several industries have produced microcogeneration systems with Stirling engines fueled by heat due to the combustion of natural gas. Among them is the WhisperGen technology, which is a residual energy system. The WhisperGen unit (**Fig. 14(B)**) has been chosen as the "world's largest residential combined heat and power facility." It is a natural gas boiler that produces hot water for domestic use and electricity A Stirling double-acting engine is coupled to an alternator. The WhisperGen unit has been studied by several researchers such as Cacabelos *et al.* [62] who propose a dynamic model of the commercial microcogeneration unit. They analyze its dynamic behavior when the engine runs at different mass flows. The transient behavior of the cogeneration unit is studied in references [63,64]. They propose a thermodynamic model that provides both electricity and energy produced.

The Stirling Thermal Motors industry, recently renamed STM Power Inc., manufactured a four-cylinder Stirling generator for cogeneration applications (**Fig. 14(C)**). The drive system of the Stirling engine is a swash plate. The Stirling engine's HEX is adjacent to a natural gas combustion chamber with a power of 55 kW.

4.6.2.5.5 Car propulsion

The Stirling engine used as a means of propelling an automobile is part of the past (but maybe also part of the future). Indeed, the Philips company studied during the years 1940 to 1980 various applications of the Stirling engine. One of these was to equip a Ford Torino, but this test was not transformed and the project abandoned. The reasons are probably related to the difficulty of having an engine capable of rapidly varying its power and speed.

In 1986, a report by NASA summarized the characteristics of the Stirling engines for the automotive industry that had been developed for this purpose, namely MOD I and MOD II, which correspond to two stages of development of a single engine. The

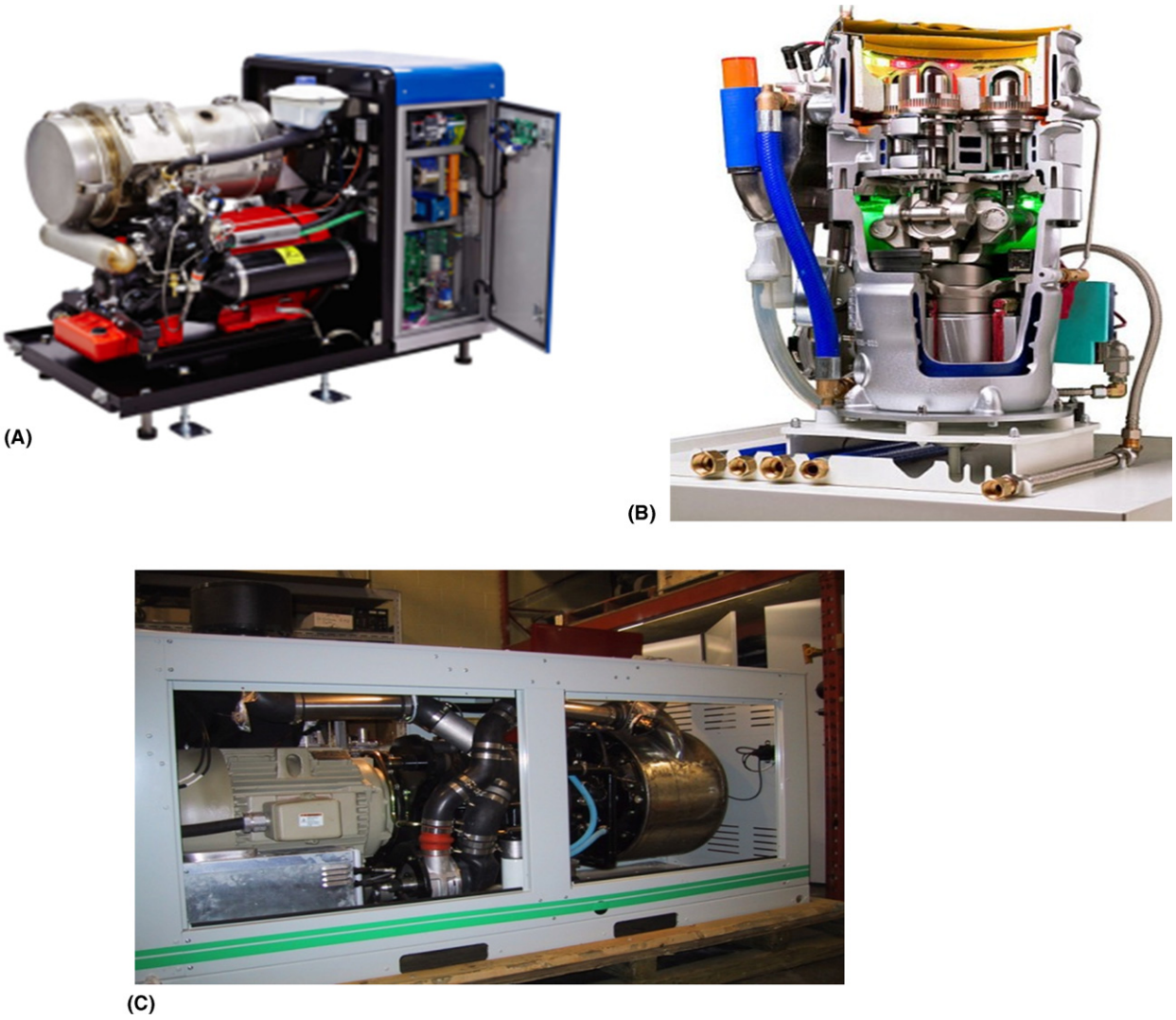

Fig. 14 Micro-CHP units using biogas or natural gas. (A) Clean energy micro-CHP unit (Biogas) (Clean Enegy. Gasbox 901 data sheet. Published online.). (B) WhisperGen micro-CHP unit "natural gas" (Reproduced from Whisper Tech Ltd. Whispergen. Product specifications. Published online.). (C) STM Power Inc. Stirling generator (Reproduced from Conroy G, Duffy A, Ayompe L. Validated dynamic energy model for a Stirling engine m-CHP unit using field trial data from a domestic dwelling. Energy Build 2013;62:18–26.).

engine used pressurized hydrogen as the working gas. It was developed and manufactured as part of collaboration between NASA and Mechanical Technology Incorporated (MTI). The MOD II engine (Fig. 15) could achieve a performance of 38.5% (much higher than the internal combustion engine (ICE): currently 20%–25% on the road and 33% in the laboratory) for comparable power to the ICE (83.5 hp = 62.3 kW).

It consumes fuel with less emission than an ICE because it burns fuel outside the engine and continuously without explosion. It thus generates much less noise in operation. As a result, it is not necessary to use a catalytic converter or silencer on the exhaust line.

Kockums developed its AIP engine during the 1980s. It has proved its worth on board the French submarine SAGA. The engine was subsequently installed on Swedish military submarines. With this system, the submarine is also able to recharge its batteries while remaining immersed. Indeed, the gases after combustion are at a pressure higher than that of the water.

Contrary to what is required of an automobile engine, an aircraft engine operates almost constantly at constant power. In this case, the Stirling engine is truly in its prime. Its silence, compared to a traditional engine, can be an asset for both the passengers of the plane and for the residents. The low vibratory level of the Stirling engine also pleads in its favor. When you take altitude, the outside air lowers in temperature. This air is the cold source of the Stirling engine. There is therefore no loss of power when one rises in amplitude. This would make it possible to fly faster than with a traditional engine. The choice of fuel being broader, one could imagine a less volatile, less explosive, and less polluting engine.

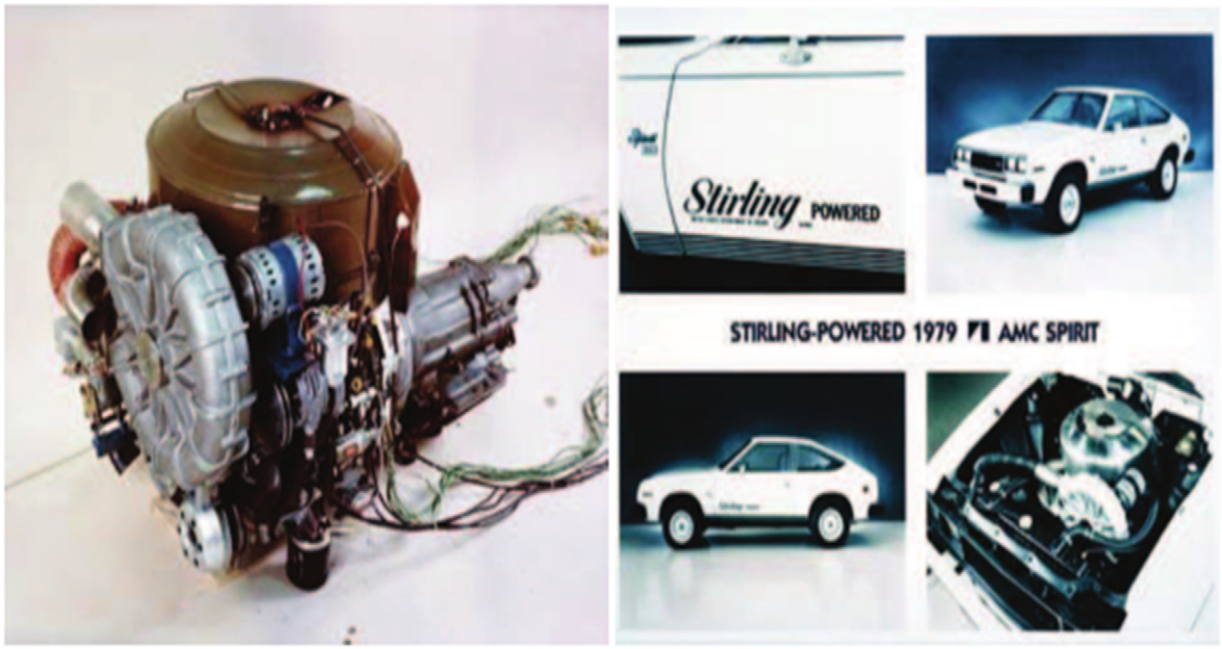

Fig. 15 The MOD II: Stirling engine used for General Motors' car and Opel prototypes. Reproduced from Autoblog. Available from: https://www.autoblog.com/2009/07/08/blast-from-the-past-nasas-stirling-powered-amc-spirit/.

4.6.2.5.6 Cold calories production

The first domestic Stirling cycle refrigeration system was studied by Finkelstein and Polonski [65]. The Stirling type V refrigerator (VISR) was developed and tested by Le'an *et al.* [66]. Parameters such as energy consumption and COP are studied at different load rotational speeds and pressures of the Stirling machine. Ataer *et al.* [67] studied numerically a Type V Stirling refrigerator using air as a working fluid. They found that when the load pressure of the machine exceeds 2 bar, the COP of the refrigerator decreases. Similarly, Giannetti *et al.* [68] studied a Stirling machine using air as a working fluid. They found that for regenerator efficiency $\varepsilon_r = 0.95$ the COP would increase to 0.77 for the top and 0.81 for the low-pressure cycle. Otaka *et al.* [69] designed and tested a Stirling type Beta machine with 100 W capacity. They studied the effect of many parameters such as the ratio of the dead volumes, the working fluid, the ratio of the volume of compression to the volume of expansion, and the phase difference between the two pistons. And they found that the refrigeration produced by nitrogen was 28% lower than that produced by helium. Recently, Formosa *et al.* [70] studied the main losses in a free-piston Stirling machine as a function of geometric and operational parameters. According to their studies, the use of the diaphragm in place of the working piston and the displacer could be a solution to the gas leak. However, the membrane will provide high thermal insulation (**Fig. 16**).

4.6.3 Regenerator Global Optimization Characteristics

Despite its small size compared to the dimensions of the Stirling engine, the regenerator porous structure has an important impact on the overall efficiency and output power of the Stirling engine. However, regenerators are very complex to model. Thus, before the modeling step, it is very important to:

- check thermophysical proprieties of the material constituting the regenerator
- determine optimal porosity value
- check the anisotropic propriety of the porous media
- choose the better conception
- identify its efficiency
- determine the effective thermal conductivity
- determine permeability
- quantify pressure drop
- check temperature inhomogeneity around the circumference of the regenerator

4.6.3.1 Constituting Material

The constituting material has a direct influence on the efficiency of the regenerator to store heat. Different materials are used as regenerator material such as stainless steel, copper, aluminum, Monel, graphite, ceramic, carbon fiber, etc. Many researches have

Fig. 16 250 We Philips Stirling Refrigerating Machine. Reproduced from WikiVisually. Available from: https://wikivisually.com/wiki/Stirling_heat_engine.

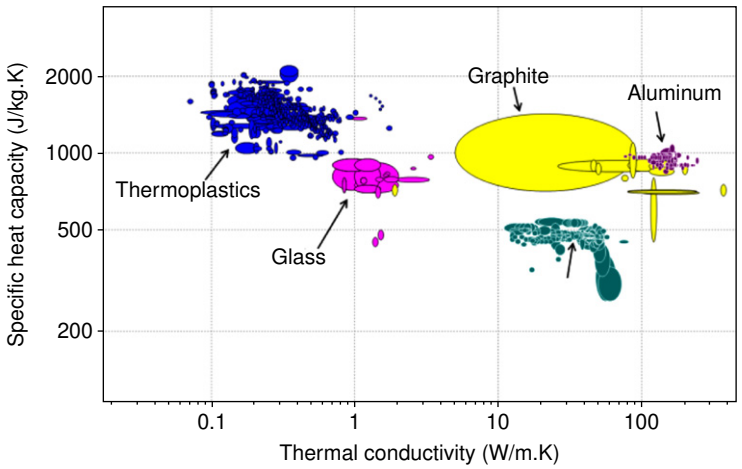

Fig. 17 Thermal conductivity and specific heat capacity of the materials used as regenerator in Stirling engines.

been made in order to identify the best regenerator material. Hofacker *et al.* [71] identified the best materials that can be used as regenerator in a Stirling engine, and they have classified them according to their thermal conductivity and heat capacity as shown in **Fig. 17**. The graphite was used for the first time as a regenerator in a Stirling engine by Hofacker *et al.* [71]. Graphite can exchange twice the amount of heat exchanged with the conventional materials used as regenerator in Stirling engines. The carbon fiber is used for the first time as regenerator material in Stirling engine by Bin Wan [18]. Carbon fiber has the characteristics of high temperature resistance, high thermal conductivity, and high corrosion resistance. The manufacturing costs are very low with long service life and the contact area between the air and the carbon fiber body is large. So, the heat transfer efficiency is high.

Abduljalil *et al.* [9] developed an experimental study to identify a low-cost material for the regenerator with performance similar to those of the materials typically used. To do this, they used a porous ceramic support, a steel sponge, a kind of stainless

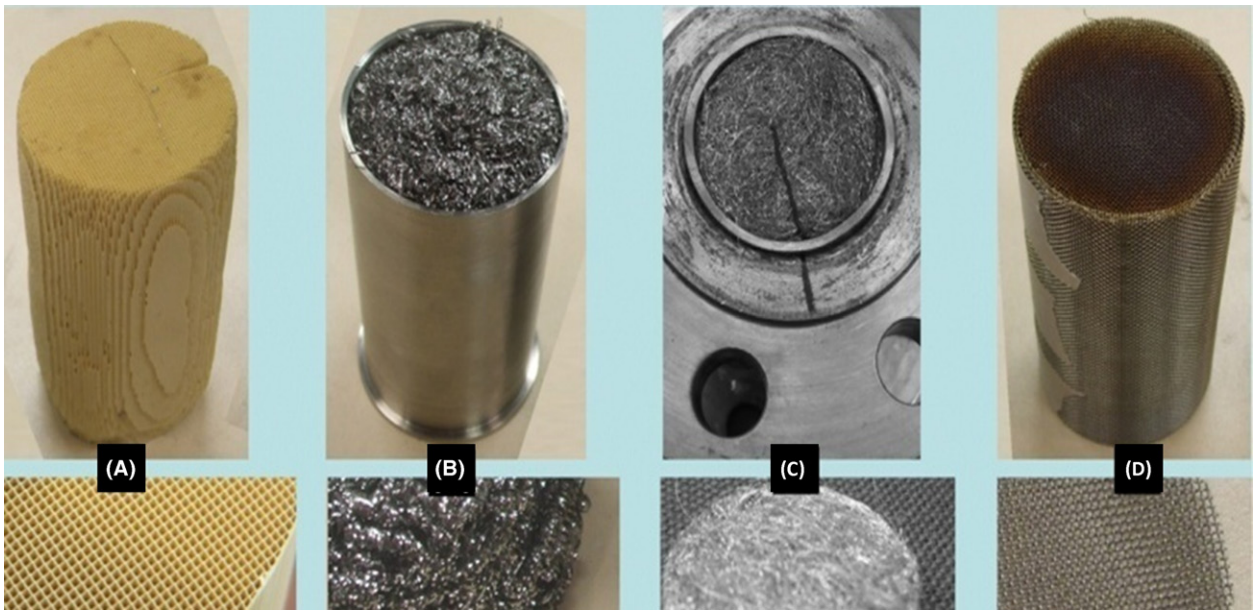

Fig. 18 Different regenerator materials: (A) ceramic catalyst support; (B) steel "scourers"; (C) stainless steel "wool," and (D) wire mesh screens. Reprinted from Abduljalil AS, Zhibin Y, Jaworski AJ. Selection and experimental evaluation of low-cost porous materials for regenerator applications in thermo-acoustic engines. Mater Des 2011;32:217–28.

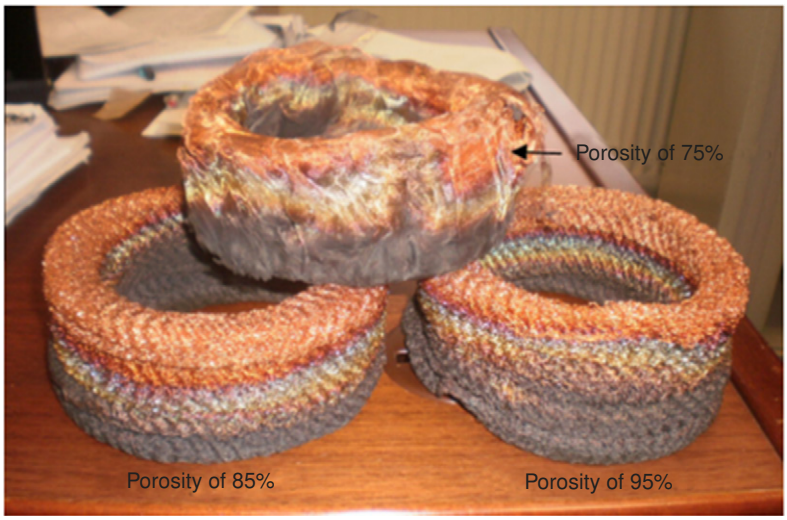

Fig. 19 Photography of copper regenerator after 15 h of experimentation.

steel wool, and finally a wire mesh screen as shown in **Fig. 18**. They tested the performance of these regenerators according to the average pressure between 0 and 10 bar. They demonstrated that the increase of the pressure drops and the flow resistance depends on the porosity, or the regularity of the porous material and the way of disposition of the solid material. Their results show that the cellular ceramics may offer an alternative to traditional regenerator materials to reduce the overall system costs.

Formosa *et al.* [20] presented theoretical and experimental studies of a GPU-3 Stirling engine. They showed that the conductivity of the material constituting the regenerator matrix has strong effect on Stirling engine performances. Gheith *et al.* [21] studied different regenerator materials and demonstrated that the Stirling engine regenerator performances are very sensitive to its material characteristics. They experiment four different regenerator materials [22,23]. These materials are: stainless steel, copper, aluminum, and Monel 400. The regenerator in Monel 400, stainless steel, and copper present the highest thermal efficiency and engine brake power. The presence of oxygen in the working fluid is a great handicap leading to the rapid oxidation of the material, and after the deterioration of its thermophysical properties and consequently the mechanical power of the Stirling engine. A photo of copper regenerator after 15 h of experimentation is presented in **Fig. 19** and marks of oxidation can be clearly seen. **Fig. 20** presents regenerators made with Monel 400 and aluminum. The aluminum regenerator has an acceptable thermal efficiency, and

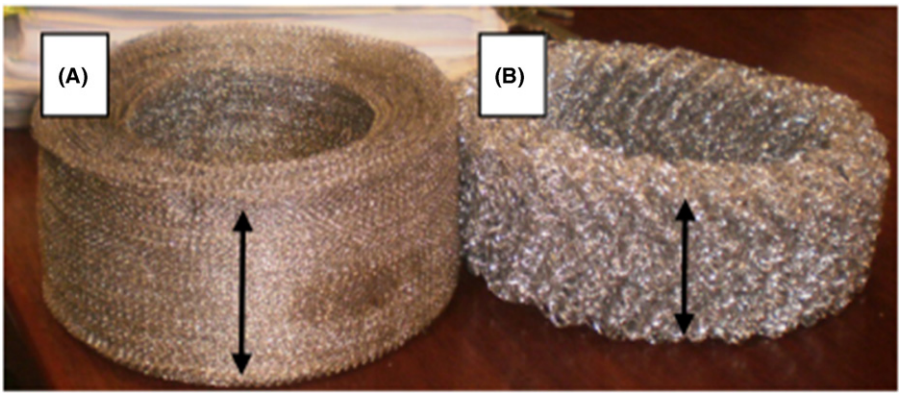

Fig. 20 Photography of the regenerator of (A) Monel 400 and (B) aluminum after 15 h of test (heating temperature under 500°C).

does not oxidize. However, its use is limited by its melting point. Gheith *et al.* [21] concluded that the stainless steel is the best material that can be used as Stirling engine regenerator working in this range of heating temperature (300°C to 550°C). According to Sadrameli [50] the use of classical material (aluminum, stainless steel, etc.) is not recommended for Stirling installation using high temperature (higher than 1000°C). At this temperature level the regenerator material must be made from ceramic with very low thermal conductivity. This dictated the effects of radial conduction in the matrix to be considerable. The dimensionless parameter that reflects this effect in packed bed heat exchangers is the Biot number.

4.6.3.2 Porosity

The porosity of the regenerator, which represents the proportion of the void in the porous part, considerably affects the performance of the regenerator to store heat. In this context, Timoumi *et al.* [72] studied the effect of porosity on thermal energy losses. They demonstrated that the reduction of porosity increases internal conduction loss and viscous friction loss as well as the dissipations by shuttle effect. But, on the other hand, it reduces losses by external convection. According to Abduljalil *et al.* [9], the high porosity of the regenerator leads to a higher thermal relaxation loss. According to the experimental studies of Gheith *et al.* [21], the optimum porosity of a regenerator constructed of stainless steel is equal to 85%. This value was considered as the most suitable matrix porosity for maximizing the Stirling engine performances and minimizing heat and friction losses. Using finite volume numerical resolution, Costa *et al.* [73] studied the effect of various structures and porosities of metal grids on the alternating flow loss.

The porosity of the regenerator is the key parameter for optimizing performance of a Stirling engine. It affects the hydraulic diameter of the regenerator, the total dead volume, the energy dissipation by pressure drops, and certainly the thermal efficiency of the regenerator and its specific exchange surface. According to Chen *et al.* [74], the use of porous material inside the Stirling engine leads to system stability. It becomes more stable to possible disturbances in the mass flow rate supply to hot fluid. The decrease in mesh porosity leads to the highest friction factor and pressure drop. In spite of the higher pressure drop we have better power and thermal efficiency because we have better heat transfer. Based on experimental studies of five stainless steel regenerators for different porosities it was found that the porosity of 85% provides the highest engine performances.

4.6.3.3 Anisotropy

The porous matrices are generally anisotropic. Several studies aim to determine the influence of this anisotropy on the hydrodynamic parameters of the flux flowing through the regenerator. Clearman *et al.* [75] experimented several types of annular porous matrices to confirm the importance of the anisotropy and the average pressure in such structures. They tested five porous structures: stacked 325 mesh screens, 400 mesh stacked screens, 400 mesh sintered screens, metal foam, alignment of micromachined nickel disks of 36–40 μm hole diameter. Recently, Tao *et al.* [76] studied numerically heat transfer in regenerator for different mesh types, materials and lengths of the porous layer. They were able to determine the anisotropic characteristics of a porous medium as regenerator in a cryogenic cooling system (PTR). The regenerator design was also deeply studied.

4.6.3.4 Conception

In order to slightly reduce the space and the weight of the engine, Eid [77] changed the classical regenerator by an alternative moving one installed inside a Beta engine cylinder. In this case, the displacer acts as a displacer and a regenerator at the same time. He concluded that a regenerator piston having a square mesh gives 20% more work and 10% more efficiency than the GPU3 engine. Andersen *et al.* [78] proposed a new conception of the regeneration matrix, divided into 3 sections. The end sections have a greater porosity and a larger wire diameter than the center section. Their new design has improved engine efficiency from 32.9% to 33.2%. Tlili *et al.* [79] studied a Stirling engine with a driving type Ross Yoke system designed for solar applications. They proposed a detailed analysis of the influence of regenerator parameters on the performance of a Stirling engine. According to them, increased porosity

leads to the decrease of the friction coefficient and the pressure drop. The effectiveness of regenerator can be changed by changing the wire diameter and length, which in turn changes the wetted surface. Xiao *et al.* [80] assumed that pressure drop per unit length decreases as the length of regenerator increases. Dietrich [81] changed the design of the regenerator to overcome the negative effects of recirculation flow and in order to improve cross thermal conductivity of the regenerator material.

4.6.3.5 Effectiveness

Referring to the major researches about the regenerator heat exchanger in the Stirling machine, it can be concluded that the most important variation of temperature, pressure, losses, and flow in the Stirling engine are observed in the regenerator (porous media, complicated heat exchange, heated and cooled at the same time). The average air temperature of the working fluid inside the regenerator is lower than its constituting material wall temperatures. Thus, many researches aim to quantify heat transfer rate through it and to determine its efficiency as shown in **Table 3**.

The regenerator effectiveness was one of the decision variables used in the multiobjective evolutionary algorithms proposed by Ahmadi *et al.* [85–87]. They proposed an optimal Pareto frontier in objective space. It was found that a final optimal solution with higher values of objectives (thermal efficiency and output power) could be achieved if the volumetric ratio and the effectiveness of the regenerator were increased. The regenerator is an imperfect heat exchanger. Number of wires and wire diameter of regenerator matrix are taken as decision variables used in parallel multialgorithms optimization by Luo *et al.* [88] to maximization of thermal efficiency and output power and minimization of power loss.

4.6.3.6 Effective Thermal Conductivity

To characterize the porous medium, the equivalent or effective thermal conductivity is an essential parameter to be determined. It depends on thermal conductivity of the constituting regenerator material λ_w, thermal conductivity of the working gas λ_g,

Table 3 Researches from literature on the regenerator effectiveness

Author(s)	*Engine type*	*Results*	*Refs.*
Ataer *et al.*	Free-piston Stirling engine	• The most important heat energy is transferred in the regenerator, which underlines its importance	[67]
Cheng *et al.*	300 W Beta-type Stirling engine with cam-drive mechanism	• The regenerator effectiveness depends on porosity, permeability, wire mesh number and material. It is also dependent on the rotational speed • When using a 120 wires mesh regenerator, the shaft power of the engine reaches 390 W at 1400 rpm with 1.21 kW input heat transfer rate (32.2% thermal efficiency)	[82]
Chen *et al.*	A c-type twin power piston Stirling engine charged with helium	• The efficiency of a moving regenerator depends on its material, matrices arrangement, matrix wire diameter, and regenerator filling factor • The regenerator efficiency had the most prominent effect on global engine efficiency, while engine rotational speed had the greatest effect on the engine output power. • The operating temperature ratio dependent on the thermal resistance of heating and cooling spaces, the effectiveness of regenerator, the working fluid mass, and the engine rotational speed	[17]
Gheith *et al.*	500-W Gamma type Stirling engine	• The selection of the appropriate regenerator constituting material is based on the recorded efficiency	[21]
Andersen *et al.*	9-kW Stirling engine	• Regenerator heat transfer rate is a very crucial factor to regenerator effectiveness especially at high engine rotational speed when the time for heat transfer is very short in each cycle • A regenerator with low heat transfer rate will perform poorly at high engine rotational speed even though it has large heat capacity	[8]
Hachem *et al.*	Beta type Stirling refrigerator	• The regenerator porosity increases beyond a critical point the Stirling refrigerator performance decreases, due to increased external conduction and lack of thermal transfer with the working fluid	[83]
Kato and Baba	Low temperature differential Stirling engine (LTDSE)	• The efficiency of the regenerator depends on the fluctuation of pressure • The temperature distribution in the regenerator is a determinant parameter of its effectiveness	[19]
Glushenkov *et al.*	Single-piston alternative to Stirling engines	• The energy efficiency is highly sensitive to regenerator performance	[84]

regenerator porosity ε, and the structure of the solid matrix. There are several calculation models of the effective thermal conductivity of a porous medium such as the effective conductivity is given by Zahi *et al.* [89] as follows:

$$\lambda_r = \lambda_g \cdot \varepsilon + (1-\varepsilon) \cdot \lambda_w \tag{22}$$

and the regenerator equivalent thermal conductivity is given as follows:

$$\lambda_r = \lambda_g \frac{\lambda_g \varepsilon + \lambda_w (2-\varepsilon)}{\lambda_g (2-\varepsilon) + \lambda_w \varepsilon} \tag{23}$$

4.6.3.7 Permeability

The permeability of a porous medium (denoted by K) characterizes the ability of the medium to allow flow there through of the fluid (liquid or gas). It depends on both the porosity and the geometry of the solid matrix. The first known permeability experiments were produced by Darcy [119] when introducing the viscosity μ of an incompressible fluid in a tube containing a porous and homogeneous medium. By measuring the rotational speed and the two pressures P_1 and P_2 respectively upstream and downstream of the porous block, Darcy has shown that there is a relationship between these pressures, Section S, height h of the tube, and the flow rate Q, which is written:

$$Q = S \frac{K}{\mu} \frac{P_2 - P_1}{h} \tag{24}$$

Permeability can be calculated using Darcy Eq. (3). However, this law is valid only for very low Reynolds number. For high speeds, inertial effects are manifested by the appearance of the term patch Forchheimer. On the other hand, it is possible to evaluate the permeability through specific geometries of the medium, means porosity, and solid matrix characteristic dimension. Such as:

Kozeny–Carman relation [90] for a simple porous medium geometry consisting of identical elements:

$$K = \frac{d^2\, \varepsilon^3}{36\, C_0 (1-\varepsilon)^2} \tag{25}$$

where d is the diameter of the constituting particles of the porous matrix and C_0 is a constant depending on the shape of particles $(3.6 < C_0 < 5)$.

Ergun relation [91] is established by considering a unidirectional flow within a porous column consisting of spherical particles of a diameter d. The column is subjected to a pressure gradient. This relation is similar to the previous relation in which $C_0 = 4.16$:

$$K = \frac{d^2\, \varepsilon^3}{150 (1-\varepsilon)^2} \tag{26}$$

When the porous matrix is modeled as a bundle of parallel capillary tubes, the expression of the permeability is:

$$K = \varepsilon \frac{d^2}{32} \text{ with } \varepsilon = \frac{n\, \pi\, d^2}{4} \tag{27}$$

where n is the number of tubes per unit area perpendicular to the direction of flow and d is the diameter of the tube.

When the permeability varies from one direction to another, the porous medium is said to be anisotropic. The permeability is characterized, in this case, by a permeability tensor.

4.6.3.8 Pressure Drops

Stirling engines are known to work under high working pressures that can reach 200 bar depending on the machine's dimensions [92]. Given its porous structure, the regenerator is the set of an important pressure drop. Many researches are made to characterize flow through a porous medium and calculate pressure drop through it. Some friction factor correlations under different working conditions are shown in **Tables 4–6**.

4.6.3.9 Temperature Distribution

Temperature distribution in both sides of the regenerator matrix is not uniform due to nonconstant fluid temperatures distribution on both the cold and hot sides. Thus, the exchanged heat in the regenerator (porous medium) is not symmetrical. Several numerical and experimental studies deal with this problem of temperature inhomogeneity on the circumference of the regenerator. Experimentally, Gheith *et al.* [21] recorded temperature distribution in the regenerator of a 500 W Gamma type Stirling engine, using eight thermocouples located in different positions of the porous matrix of the regenerator and arranged in a symmetrical manner. Their results show the axisymmetric evolution of temperature reduces the efficiency of regenerator to store calories. Dietrich [81] assumes a temperature inhomogeneity around the circumference of the regenerator of a Stirling pulse tube (PTC). He concluded that regenerator temperature inhomogeneity depends on the temperature gradient, on the mass flow, and on the transverse thermal conductivity of the material constituting the regenerator.

Table 4 Summary of friction factor correlations for monophasic flow through a porous medium

Author(s)	*Friction factor correlation*		*Conditions*
Ergun [91]	$\frac{1-\varepsilon}{\varepsilon^3}\left(\frac{150}{Re}+1.75\right)$	(28)	$\varepsilon<0.8$ $Re<3000$
Macdonald [93]	$\frac{1-\varepsilon}{\varepsilon^3}\left(\frac{150}{Re}+b\right)$	(29)	$b=1.8$ (Smooth particles) $b=4$ (rugged particles)
Hicks [94]	$6.8Re^{-0.2}\frac{(1-\varepsilon)^{1.2}}{\varepsilon^3}Re^{-0.2}$	(30)	$500<Re<6000$
Rose and Rizk [95]	$1000Re^{-1}+125Re^{-0.5}+14$	(31)	$1000<Re<6000$
Tallmadge [96]	$\frac{1-\varepsilon}{\varepsilon^3}\left(\frac{150}{Re}+\frac{4.2}{Re^{1/6}}\right)$	(32)	$0.35<\varepsilon<0.88$ $0.1<Re<10^5$
Lee and Ogawa [97]	$6.25\frac{(1-\varepsilon)^2}{\varepsilon^3}\left(29.32Re^{-1}+1.56Re^{-n}+0.1\right)$	(33)	$n=0.352+0.1\varepsilon+0.275\varepsilon^2$ $1<Re<10^5$

Table 5 Theoretical assumptions for models

Isothermal model	*Adiabatic model*	*Quasi-steady model*
• The gas in the expansion space and the heater is at the highest temperature, and the gas in the compression space and the cooler is in the lowest temperature • The total mass of the gas engine is constant. The fluid used is assumed to be perfect for this we apply the equation ideal gas • For the assumed linear temperature distribution in the regenerator, the effective regenerator temperature T_r is given by: $T_r=\frac{(T_h-T_k)}{ln\left(\frac{T_h}{T_k}\right)}$ • Each compartment is considered a homogeneous entity represented by the gas mass m, its absolute temperature T, its volume v, and pressure P • In this ideal model, the losses are neglected: while the pressure P is the same in all compartments	The working spaces are assumed adiabatic The conditional temperatures caused by the discontinuity of those between workspaces is introduced, are also considered nonideal	• The heater and cooler wall temperatures are maintained constants at: T_{Wh} and T_{Wk} • The working fluid temperature is different from those of the heat exchanger wall • The heat exchanger temperature isn't constant, those of the compartments interfaces too • The regenerator is subdivided into two cells r1 and r2 • The outflow direction is arbitrarily defined from the compression space toward the expansion one. **Fig. 1** schematizes the distribution to be theoretically studied The dynamic model takes also into consideration the frictional drag force, which gives rise to a pressure drop across each heat exchanger component as well as a corresponding flow dissipation internal heat generation effect

4.6.4 Numerical and Theoretical Simulation of Stirling Engine Regenerator

4.6.4.1 Global Theoretical Modeling

Three theoretical models are usually used. The isotherm analysis is the easiest to develop. It was proposed by Gustave Schmidt. The Stirling engine power is based on an ideal analysis. A simple correction factor is then used to deduce the real mechanical power from the ideal one. The second model is the adiabatic model that was developed by Finkelstein [65]. The third model is the quasi-stationary model. The major difference between this model and the adiabatic model is that the gas temperature is not equal to the temperature of the walls of the associated heat exchanger [98,99].

4.6.4.2 Losses in Regenerator

4.6.4.2.1 Internal conduction loss

An important gradient of temperature between Stirling engine interfaces leads to an internal conduction loss through the regenerator. This letter is divided in two sections (hot one: near the heater and cold one: near the heater). This loss is calculated

Table 6 Comparison between theoretical models and experimental results

Engine	*Isothermal model*	*Adiabatic model*	*Quasi-steady model*	*Quasi-steady model + losses*	*Experimental results*
Brake power (W)	632.97	438.42	284.70	272.73	273.90
Thermal efficiency (%)	62.8	56.9	37.2	22.8	23
Remarks	• High power and efficiency • Non-acceptable results • poor model	• High power and efficiency • Nonacceptable results • Poor model	• Low power and efficiency • Acceptable results • Good model	• Low power and efficiency • Acceptable results • Very good model	• Low power and efficiency

within the two sections of the porous matrix as follows [100]:

$$\delta\dot{Q}_{\mathrm{Cdr2}} = \frac{\lambda_{\mathrm{m}} A_{\mathrm{r2}} (T_{\mathrm{r2-h}} - T_{\mathrm{r1-r2}})}{L_{\mathrm{r2}}} \tag{34}$$

$$\delta\dot{Q}_{\mathrm{Cdr1}} = \frac{\lambda_{\mathrm{m}} A_{\mathrm{r1}} (T_{\mathrm{r1-r2}} - T_{\mathrm{k-r1}})}{L_{\mathrm{r1}}} \tag{35}$$

The regenerator thermal conductivity depends on the porosity ϕ, on the thermal conductivity of the working fluid λ_{g} and of the material λ_{m}. It can be calculated as [92]:

$$\lambda_{\mathrm{r1,r2}} = \lambda_{\mathrm{g}} \frac{\lambda_{\mathrm{g}}\phi + \lambda_{\mathrm{m}}(2-\phi)}{\lambda_{\mathrm{g}}(2-\phi) + \lambda_{\mathrm{m}}\phi} \tag{36}$$

4.6.4.2.2 Loss due to regenerator imperfection ε_r

The regenerator material stores energy from the hot gas and restores it during its passage in the opposite direction toward the cooler. The amount of heat stored or restored by the regenerator matrix depends on the characteristics of the material. This loss can be illustrated by the regenerator thermal efficiency ε_{r}, expressed as follows:

$$\varepsilon_{\mathrm{r}} = \frac{\mathrm{NTU_r}}{1 + \mathrm{NTU_r}} \tag{37}$$

So, the effective thermal power exchanged in the Stirling engine regenerator is $\dot{Q}_{\mathrm{irr}}$, calculated as follows:

$$\dot{Q}_{\mathrm{irr}} = (1 - \varepsilon_{\mathrm{r}})\dot{Q}_{\mathrm{r}} \tag{38}$$

4.6.4.2.3 Friction loss in heat exchangers $\delta\dot{Q}_v$

The fluid friction associated with the flow through the porous media will result in a pressure drop, Δp, across the three heat exchangers, which greatly reduces efficiency and power output of the engine. To evaluate pressure, drop through heat exchangers, we use this correlation:

$$\Delta p = -\frac{2f\mu u V}{D d_{\mathrm{hyd}}^2} \tag{39}$$

The energy power loss ($\delta\dot{Q}_{\mathrm{vr}}$) through the porous media due to pressure drop in the heater regenerator is expressed as follows:

$$\delta\dot{Q}_{\mathrm{vr}} = -\frac{\dot{m}_{\mathrm{r}} \Delta p}{\rho_{\mathrm{m}}} \tag{40}$$

4.6.4.3 Model Comparison

For the same conditions: $T_{\mathrm{h}} = 500^{\circ}\mathrm{C}$, $T_{\mathrm{K}} = 303\mathrm{K}$, $N = 390$ rpm, and $P_{\mathrm{i}} = 5$ bar the following performances for a Gamma type Stirling engine are obtained.

4.6.4.4 Computational Fluid Dynamics Simulations

CFD simulation has gained important interest to treat engineering problems. CFD is concerned with numerical solution of differential equations governing transport of mass, momentum, and energy in moving fluids. In Stirling engine, CFD can be used to study flow, heat transfer, pressure, and losses inside the whole engine. For this, the geometry and the mesh model representing

the real installation are created and then initial and boundary conditions are defined. Finally, the movement of hot and cold room pistons are added to the simulation. CFD approach allows the heat transfer characteristics to be investigated in great detail. Results describe the behaviors of temperature, pressure and velocity in different spaces and especially in the regenerator. The effect of regenerator properties is investigated. The impact of the porosity on convective heat transfer inside the regenerator is deduced. A comparison between three regenerator materials is presented and the better material assuming good temperature gap between hot and cold rooms is deduced.

Recently, studies based on computational fluid dynamics (CFD) optimize the Stirling engine performances and tested new installations (cogeneration, recovery systems, etc.). Zhigang Li *et al.* [101] simulated flow and heat transfer in a compact porous-sheets heat exchanger. They found that the porous-sheets regenerator has 38%–51% lower total entropy generation rate, thus leading to less available work loss, contributing to higher power output and thermal efficiency compared to the conventional wire mesh regenerator. Jose Leon *et al.* [102] studied, with a very simple design and geometry, heat transfer characteristics of a β-type Stirling engine. It is found that impingement is the major heat transfer mechanism in the expansion and compression chamber and temperature distribution is highly nonuniform across the engine at any given moment. Wen-Lih Chen *et al.* [103] studied heat transfer characteristics of a twin-power piston γ-type Stirling engine. They proved that using a moving regenerator can enhance the performance of a β-type Stirling engine. The moving regenerator acts as an effective thermal barrier between both working spaces causing the reduction in rates of heat input and output and increasing of the engine's indicated power. Using three-dimensional numerical simulations, Costa *et al.* [104] characterize heat transfer and pressure drop phenomena through both stacked and wound woven wire matrix regenerator under different porosity and flow boundary conditions. They present new Nusselt number correlation equations applied to characterize and hence to optimize stacked and wound woven wire Stirling regenerator.

4.6.4.4.1 Turbulent models

The flow inside the Stirling engine is turbulent, hence the choice of a turbulence model. The turbulence modeling consists in representing either the influence of turbulence on the average flow (statistical approaches of the RANS type), or the influence of the unresolved scales on the solved scales (filtered approaches of the large eddy simulation: LES). RANS stationary models are used to obtain a good approximation of average values in industrial flows. The main RANS models available are listed in **Table 7**.

4.6.4.4.2 Case 1: Computational fluid dynamics simulation of a 25 W Beta type Stirling engine

A CFD model is developed to simulate flow and heat transfer across Beta type Stirling engine singularities. CFD approach allows the heat transfer characteristics to be investigated in great detail. Results describe the behaviors of temperature, pressure, and velocity in different spaces. The effect of regenerator proprieties is investigated. The impact of the porosity on convective heat transfer inside the regenerator is deduced. A comparison between three regenerator materials is presented and the better material assuming good temperature gap between hot and cold rooms is deduced.

The geometry of a Beta type Stirling engine is represented in **Fig. 21**. Its geometric characteristics are given in **Table 8**. The Stirling engine is composed of three parts: the warm space, the porous medium, and cold space; the geometry is devised into three distinct parts connected when creating interfaces between the porous medium and hot and cold rooms.

Air (ideal gas) is selected as working fluid and copper as regenerator material. Operating pressure is chosen to be 101,325 Pa. As boundary conditions, the regenerator is chosen to be porous region with adiabatic walls having two interfaces, one hot side and

Table 7 Statistical models of turbulence type RANS

Models	*Advantages*	*Inconvenient*
Spalart-Allmaras	Economic (Eq. (1)). Good for free flows, and flows on profile without detachments or large pressure gradients	Requires a higher resolution of the mesh at the borders (no laws on the walls)
Standard k-epsilon	Robust, economical and relatively precise. Suitable for flows with large Reynolds number	Mediocre results for complex flows (strong pressure gradient, rotation, and swirl)
RNG k-epsilon	Derived by a rigorous statistical method. Good for moderately complex flows (jet impact, flow separation, and recirculation)	Limited by the hypothesis of isotropic turbulent viscosity
Realizable k-epsilon	Respect a physical constraint that can violate the model k-epsilon. Offers the same benefits as the RNG. Recommended in the case of turbomachines	Limited by the hypothesis of isotropic turbulent viscosity
SST and Standard k-Omega	Model recommended for turbine engine problems (compare to realizable k-epsilon). The SST k-omega version consists of a transition between the standard k-omega model (developed for moderate Reynolds numbers and boundary layers) and the high Re version of k-epsilon when far from the walls	Requires a higher resolution of the mesh at the borders (no laws on the walls)
Reynolds stress model (RSM)	The most physically complete model (transport and anisotropy of turbulence are taken into account)	Requires more CPU time. The equations of momentum and transport of turbulence are closely related

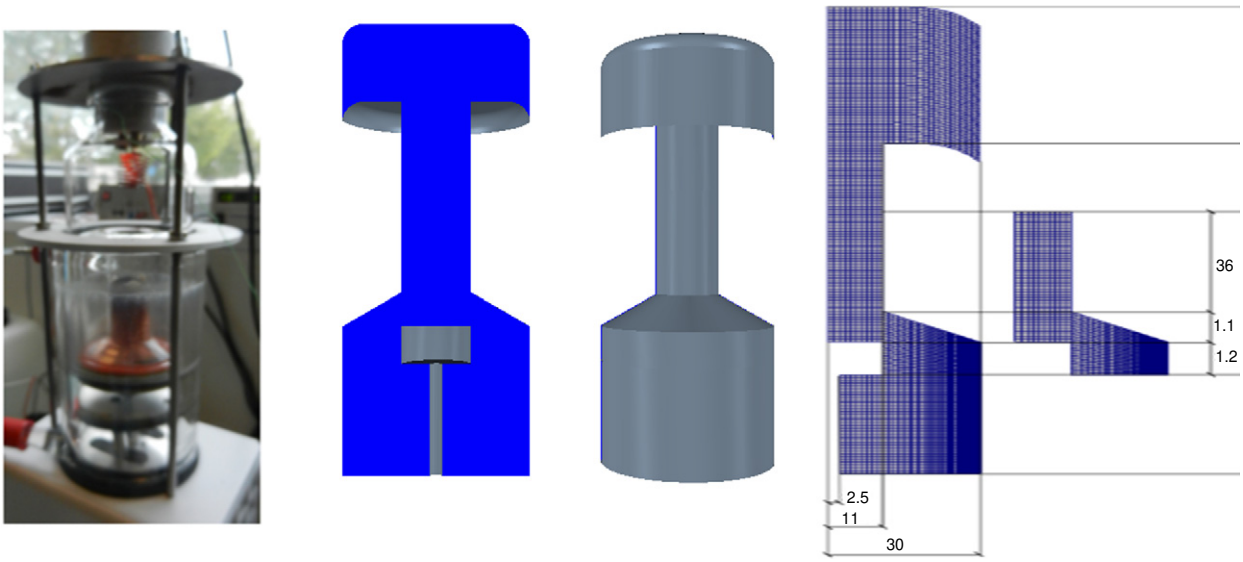

Fig. 21 Beta type Stirling engine. (A) Experimental prototype. (B) Geometry. (C) Dimensions.

Table 8 Geometrical properties of the experimental engine

Hot space diameter [mm]	60
Hot space height [mm]	49.2
Displacer con rod length [mm]	100
Displacer stroke [mm]	48
Cold space diameter [mm]	60
Cold space height [mm]	35.7
Power piston con rod length [mm]	197
Power piston stroke [mm]	48
Regenerator inner diameter [mm]	22
Regenerator outer diameter [mm]	60
Regenerator height [mm]	59
Regenerator porosity	0.79
Maximum machine volume [cm^3]	300
Minimum machine volume [cm^3]	160

one cold side. Hot space is chosen to have isothermal walls, maintaining at a constant temperature of 700K. The cold space walls are maintained at a constant temperature of 300K. And hot and cold pistons are chosen to be adiabatic.

Fig. 22 represents the repartition of temperature obtained by the CFD simulation. Isothermal curves for two different crank angle values can be seen. The highest temperature is observed at the expansion space while the lowest temperature is recorded at the compression space. The temperature inside the regenerator increases linearly as we are closer to the hot space. During compression isotherm curves are entrained by the direction of the moving pistons. Temperature distribution inside the Stirling engine does not have a symmetric distribution due to turbulence. It is clearly seen that during expansion, the diffusion of the hot heat flux becomes less important than the distribution of cold heat flow. This can be explained by the fact that the velocity of the flow during the compression is much greater than during expansion.

Instantaneous variation of temperature and pressure can be obtained by CFD simulation too (Figs. 23 and 24). Very precise variation can be observed. The pressure difference among the two spaces can be attributed to the internal pressure drop of the gas passage through the regenerator. Despite its ability to transfer heat, the porous structure of the regenerator also acts as a barrier to the gas following the compression and expansion spaces. This can be seen from the variation of pressure in Fig. 8. Here the pressure difference is defined as $\Delta p = P_{\text{compression}} - P_{\text{expansion}}$. In the case with 10 Hz of operating frequency, the average frictional pressure drop in the regenerator is about 0.1 bar.

Fig. 25 shows the 2D velocity vectors at different crank angles. It can be seen that velocity of the working fluid through the regenerator is higher than other compartments.

At the beginning of the compression phase ($\theta = 36$ degree), the velocity vectors are parallel to the symmetry axis. When the fluid particles are accelerated ($\theta = 180$ degree), there is a strong deviation of the velocity vector. The behavior of working fluid particles

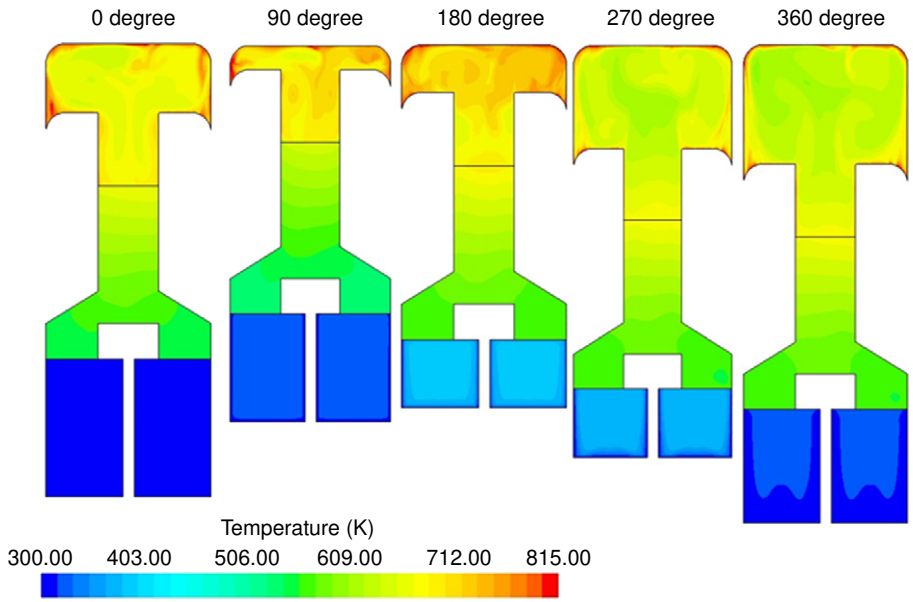

Fig. 22 Temperature contour of Beta type Stirling engine during a computational fluid dynamics (CFD) simulation at different crank angle.

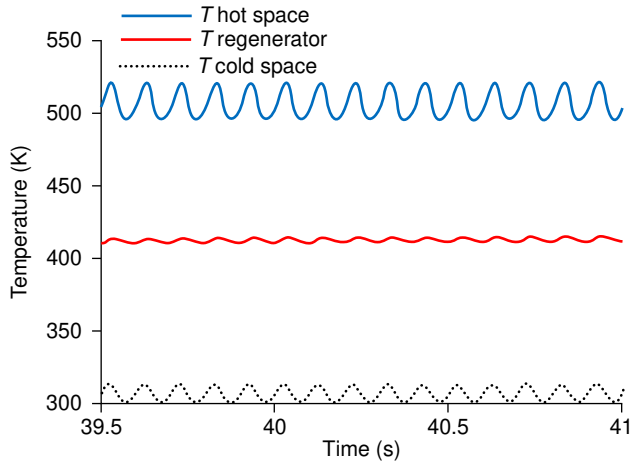

Fig. 23 Average temperature evolution in each space vs. time.

can be seen. For $\theta = 216$ degree, two recirculation zones in the regenerator are observed. This is explained by the separation phenomenon of the boundary layer and by the pressure drop generated by the porous block, which causes the formation of a vortex.

The most important parameters of a Stirling engine regenerator are its material and its porosity. Both parameters can be investigated through a CFD simulation. The Nusselt number evolutions versus operation time for two regenerator porosities are presented in **Fig. 26**. The porosity increase leads to the working fluid velocity inside the porous region, which ameliorates convective heat transfer and consequently increases the Nusselt number.

The copper, aluminum, and stainless steel temperature coefficients versus operation time are presented in **Fig. 27**. It can be seen that the aluminum is heating faster and the cooler is heating lower. So, aluminum is the faster material that attains the quasi-steady state but it is the worst material that can separate between hot and cold spaces, which deteriorate the regenerator efficiency.

4.6.4.4.3 Case 2: Computational fluid dynamics simulation of a 1 kW double acting type Stirling engine

The double acting Stirling engine of the WhisperGen boiler was considered to simulate the flow and heat transfer inside the Stirling engine. Geometric characteristics of this engine are shown in **Table 9**. CFD simulation results show the variation of pressure, temperature, and velocity during a cycle. The effect of the regenerator porosity on the mechanical power was investigated.

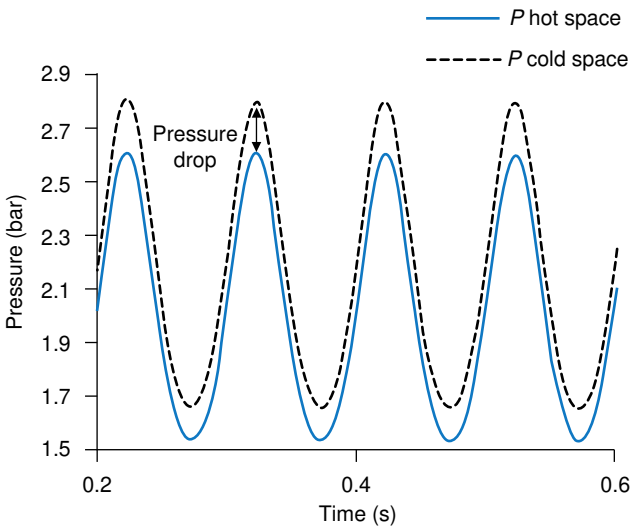

Fig. 24 Periodic evolution of the average pressure at hot and cold spaces at steady state when $f=10$ Hz.

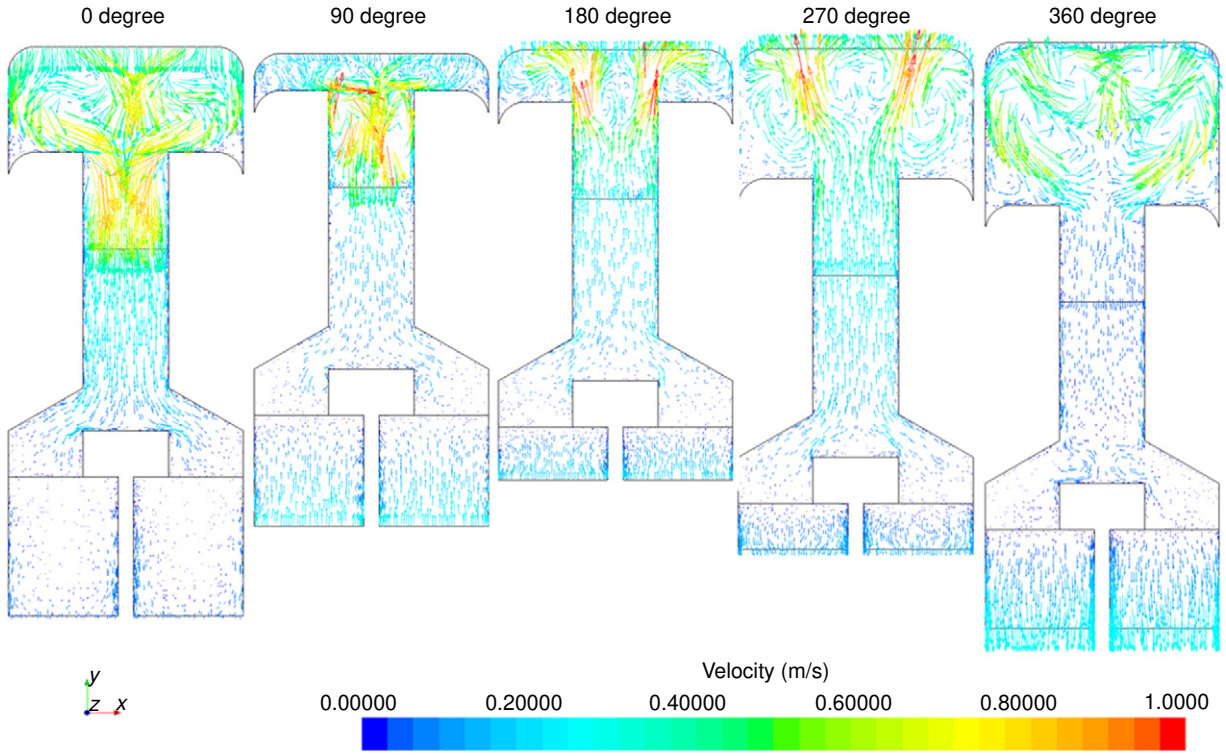

Fig. 25 Velocity vector diagram of the fluid through the regenerator at different crank angle.

The double acting Stirling engine consists of four cylinders. The geometry of one cylinder is considered in the CFD simulation. The simulated geometry is devised into five different regions as shown in **Fig. 28**: Hot region (expansion space + hot canals), regenerator and finally cold region (compression space + cold canals).

1. Pressure, temperature, and velocity: the pressure in the regenerator remains as the mean pressure between the hot and cold chamber and it is represented by the green color (**Fig. 29(A)**).

According to **Fig. 29(B)**, it is clearly seen that the maximum temperature is in the hot chamber domain. The red color represents temperature around 1000K, the yellow color in the interface between the regenerator and the hot canals shows that the temperature rises in that side from 785K to 900K and on the other hand the interfaces between the regenerator and the cooler shows

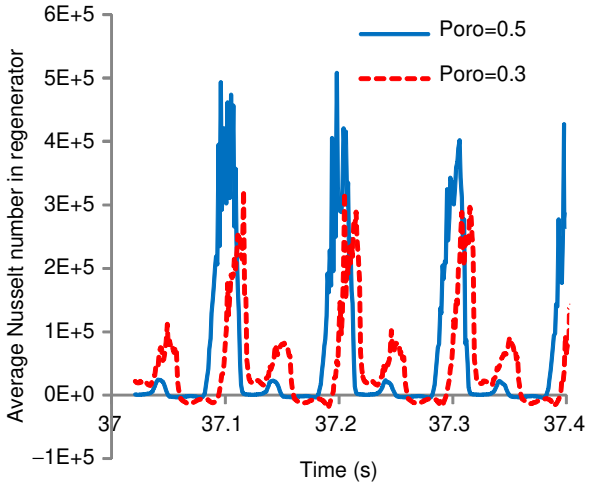

Fig. 26 Average Nusselt number evolution vs. time for different regenerator porosity.

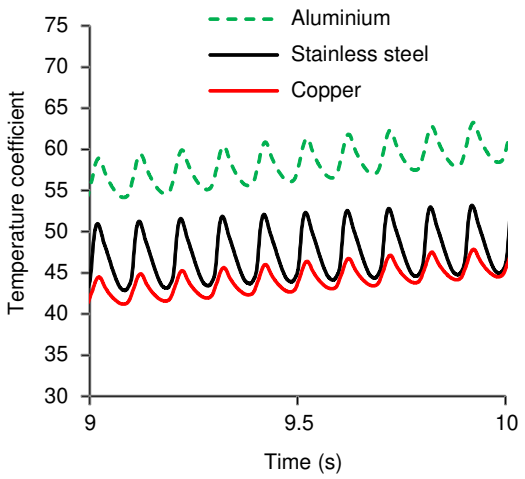

Fig. 27 Temperature coefficient evolution versus time for different regenerator material.

Table 9 Geometry values of input data for the simulation

Geometry parameters	*Values*
Engine piston number	4
Piston diameter (cm)	4.34
Displacement volume (cm^3)	64
Expansion space volume (cm^3)	33.85
Compression space volume (cm^3)	30.11
Regenerator volume (cm^3)	22.11
Expansion space phase angle advance (degree)	180
Rotational speed (Hz)	25
Wire matrix diameter (m)	6E-5
Matrix screen width (m)	2.16E-04

the existence of light blue color, which is in the middle between the dark blue color of the cooler temperature and the green color of the regenerator, which shows that the heat exchange between the regenerator and the cooler is taking place in the simulation, thus the regenerator works as a heat exchanger between the two chambers not only to prevent thermal shock but also to fasten the heat process of the hot chamber to get hotter and of the cold chamber to get cooler, which will end up raising the engine efficiency.

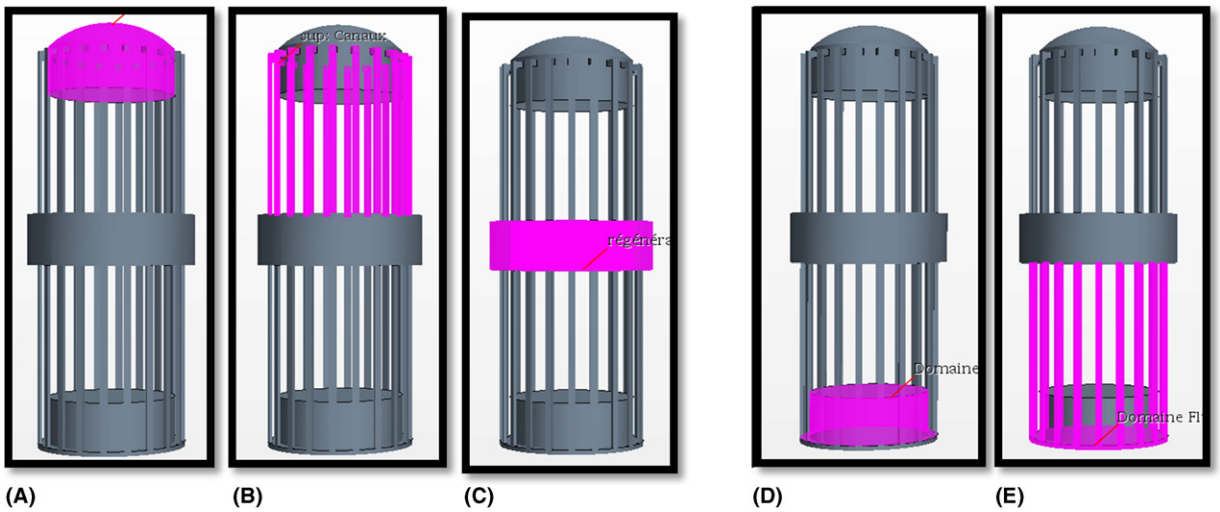

Fig. 28 Geometry investigated for the numerical computational fluid dynamics (CFD) simulations. (A) Expansion space boundary. (B) Hot canals boundary. (C) Regenerator boundary. (D) Compression space boundary. (E) Cold canals boundary. Reproduced from Gheith R, Frikha M, Hachem H, Aloui et F, Ben Nasrallah S. Simulation CFD des échangeurs de chaleur dans un moteur Stirling à Double effet, Proceeding Journées Internationales de la Thermique, JITH 2017, Monastir, Tunisia; 2017.

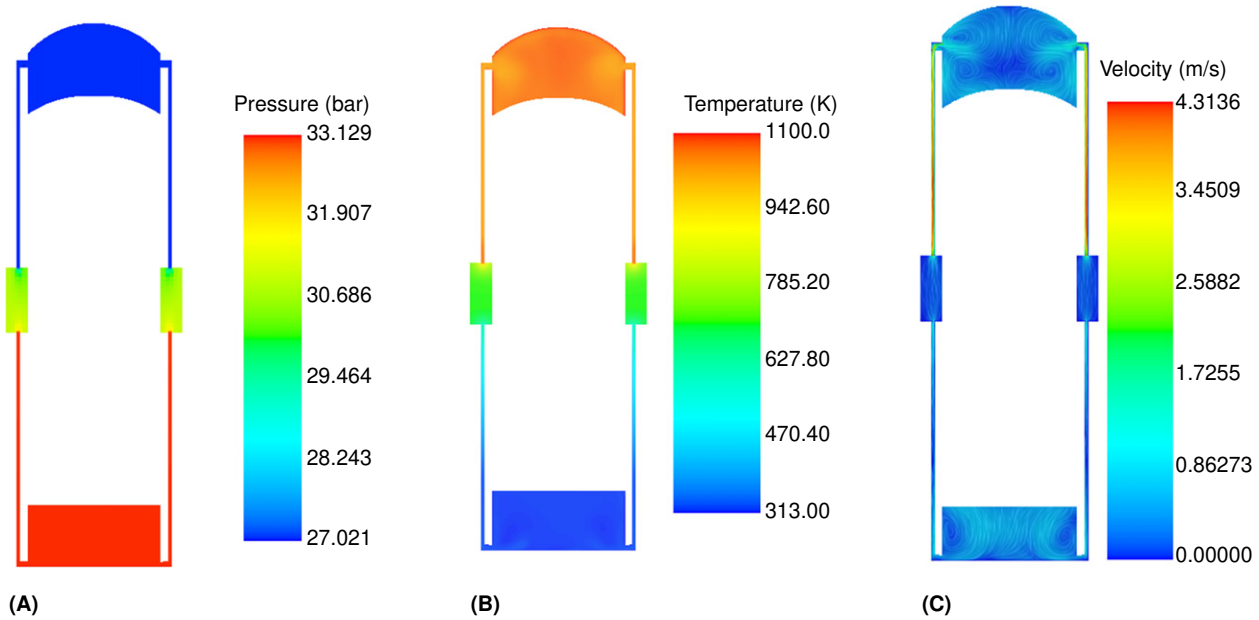

Fig. 29 Distribution of (A) pressure, (B) temperature and (C) velocity. Reproduced from Gheith R, Frikha M, Hachem H, Aloui et F, Ben Nasrallah S. Simulation CFD des échangeurs de chaleur dans un moteur Stirling à Double effet, Proceeding Journées Internationales de la Thermique, JITH 2017, Monastir, Tunisia; 2017.

The working fluid velocity in the canals are high, presented by the red color, because the canal is too small and the heating process takes less time so the temperature increases, which increases the pressure and results in increasing the working fluid velocity in the canals. The working fluid velocity decreased from 3 m/s in the canals part to 1 m/s in the regenerator pores and 0 m/s in other point of the regenerator (Fig. 29(C)). Four vortexes were formed due to the incoming fluids from the canals with high velocity and temperature spread in the expansion hot chamber, in fact the hot fluid (1100K) is mixed with the coming cold fluid from canals. However, in the compression cold chamber, there are only two vortexes, in fact the fluid leaves the regenerator at about 670K of temperature and starts the cooling process.

The change of surface between canals and chambers causes not only pressure drop but also turbulence in the fluid flow, which leads to the formation of vortexes. The vortex apparition enhances the heat transfer between walls and fluids.

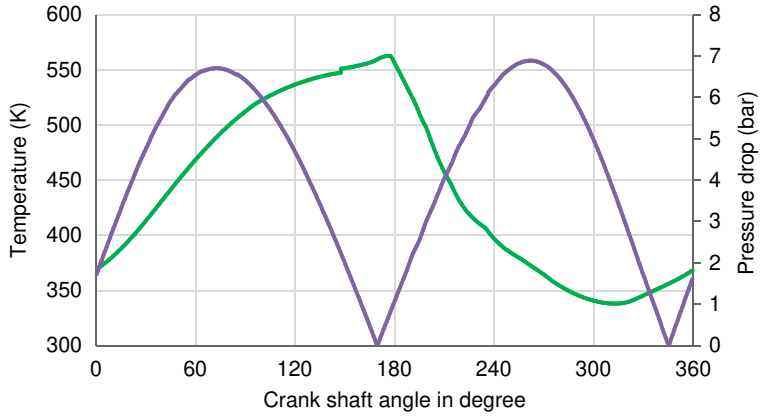

Fig. 30 Regenerator velocity and pressure drop evolution with crank shaft angle ($\Delta\phi = 100$ degree). Reproduced from Gheith R, Frikha M, Hachem H, Aloui et F, Ben Nasrallah S. Simulation CFD des échangeurs de chaleur dans un moteur Stirling à Double effet, Proceeding Journées Internationales de la Thermique, JITH 2017, Monastir, Tunisia; 2017.

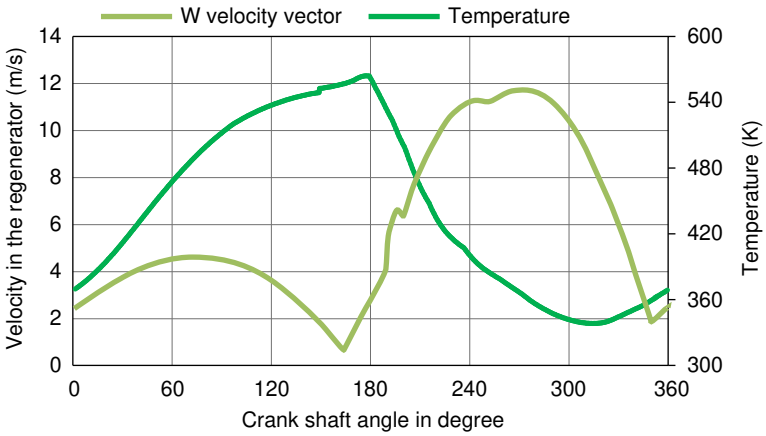

Fig. 31 Regenerator velocity and temperature evolution with crank shaft angle ($\Delta T = 126$ degree). Reproduced from Gheith R, Frikha M, Hachem H, Aloui et F, Ben Nasrallah S. Simulation CFD des échangeurs de chaleur dans un moteur Stirling à Double effet, Proceeding Journées Internationales de la Thermique, JITH 2017, Monastir, Tunisia; 2017.

2. Regenerator temperature and pressure drop: **Fig. 30** shows that the maximum regenerator temperature corresponds to the minimum pressure drop. In fact, pressure drop is highly related with energy dissipation, between expansion and compression phases the flow changes its directions, velocity in that moment equals zero, and hence the pressure drops equal zero, at that moment the viscous dissipation related to the flow movement is equal to zero, which means the temperature rises as the velocity decreases.

The pressure drop is more important in the middle of expansion and in the middle of compression phase, at these two moments the regenerator pressure reaches a maximum value.

3. Regenerator temperature, pressure drop and velocity: during the expansion phase between 0 and 180 degrees the pressure in the hot chamber increases, and its volume decreases. Thus, the regenerator starts stocking the heat coming from the fluid going through it from hot chamber through canals to the regenerator.

During the compression phase, as the piston start to move from 180 to 360 degrees the regenerator exchanges heat with both sides, with cold chamber in order to prevent thermal shock of the engine and with the hot side preparing for the next cycle in order to save energy, and that's why the regenerator temperature decreases (**Fig. 31**).

This phenomenon is similar to the electrical behaviors of capacitors while charging and discharging due to presence of electrical resistances in the electrical circuit. In the Stirling engine a similar phenomenon occurred in the regenerator due to presence of two resistances: the viscous resistance and the inertial resistance (**Fig. 32**).

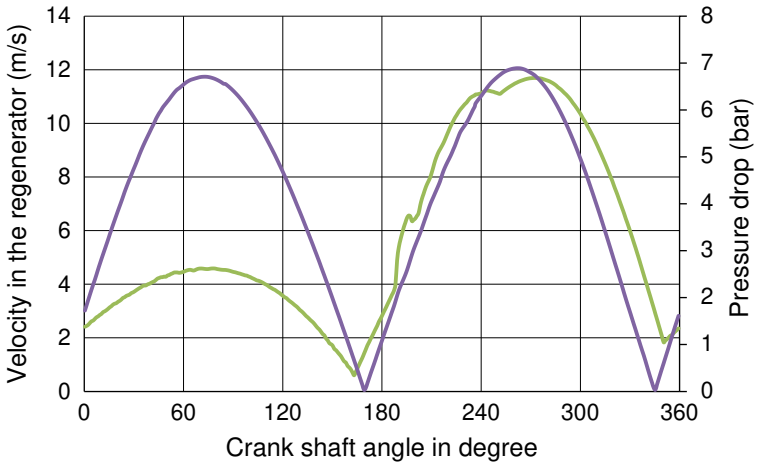

Fig. 32 Regenerator velocity and pressure drop evolution with crank shaft angle ($\Delta\phi = 6$ degree). Reproduced from Gheith R, Frikha M, Hachem H, Aloui et F, Ben Nasrallah S. Simulation CFD des échangeurs de chaleur dans un moteur Stirling à Double effet, Proceeding Journées Internationales de la Thermique, JITH 2017, Monastir, Tunisia; 2017.

Table 10 Regenerator inertial resistance and viscous resistance at different porosity

Porosity	*Inertial resistance* R_{vz}	*Viscous resistance* R_{iz}
0.65	1.8586e + 10	7.4344e + 04
0.725	8.2688e + 09	4.2095e + 04
0.85	1.5266e + 09	1.4248e + 04
0.95	1.2149e + 08	3.4019e + 03

Table 11 Comparison between figure of merit (FOM) formulations from literature

F_{M1} *(Eq. (43))*	F_{M2} *(Eq. (44))*	F_{MSC} *(Eq. (45))*
Includes the heat transfer and the thermal dispersion (denominator terms)	Includes the thermal energy transport (enthalpy + dispersion) and the pumping power	Does not include the regenerator flow area. Inclusion of the dead volume ration as defined below:

4. Effect of regenerator porosity: based on Ergun equation (Eq. (28)), we are able to introduce the two principal parameters for the porous media simulation, which are the viscous resistance and inertial resistance as follows:

$$R_{\mathrm{i}} = \frac{(1-\varepsilon)^2 * 150}{\varepsilon^3 Dp^2} \tag{41}$$

$$Rv = \frac{(1-\varepsilon)}{\varepsilon^3 Dp} * 1.75 \tag{42}$$

When varying only porosity and making all other parameters constant, the inertial resistance and the viscous resistance of the regenerator are calculated according to Eqs. (41) and (42) as shown in **Tables 10** and **11**.

Effect of regenerator porosity on output mechanical power of the double acting Stirling engine is investigated. **Fig. 33** shows that the highest output mechanical power (about 1.4 kW) is obtained when the regenerator porosity is about 0.775.

The regenerator porosity and matrix wire diameter are critical parameters for the Stirling engine performance. High matrix porosity values lead to high regenerator effectiveness but low engine performance. An increase of the matrix heat capacity leads to the reduction of the engine's performance, the torque as well as the work output.

The regenerator temperature profile of the working fluid is related to position and time. The nonideal behavior of the regenerator is demonstrated and the remaining heat in the regenerator grid is recorded when the thermal equilibrium is achieved.

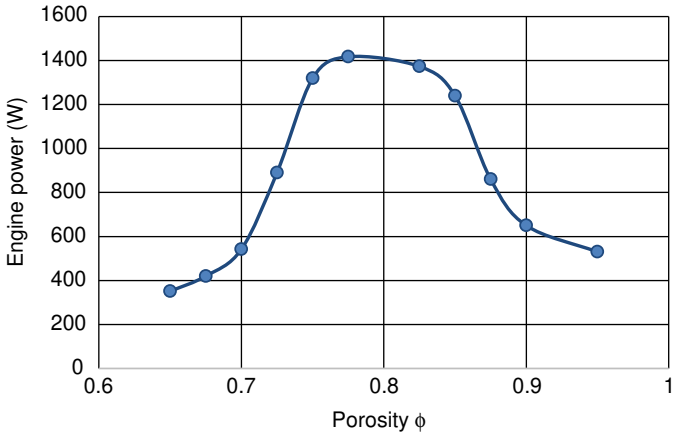

Fig. 33 Evolution of the power output with the porosity for $P_i = 20$ bar, $T_h = 1100$K, and $T_k = 313$K.

4.6.5 Experimental Studies of Stirling Engine Regenerators

4.6.5.1 Figure of Merit Formulation

The figure of merit (FOM) is considered as a powerful tool to determine adequate Stirling engine regenerator. The FOM allows comparing different ratio for the tested regenerators at the same time. A regenerator with a $F_M = 1$ is an ideal regenerator (no losses).

Ibrahim *et al.* [105] proposed a regenerator steady based on FOM formulations. They found that the microfabricated regenerator has a higher F_M than woven screen or random fiber matrices. The FM is in the range of 0.07–0.42 when the Reynolds number is 10–1000. The FOM is useful to compare several regenerators for the same Stirling engine and does not track overall engine efficiency.

Initially the formulation of the FOM was proposed by Gedeom [106–108] (Eq. (43)), then it was ameliorated by Ibrahim *et al.* [105] (Eq. (44))

$$F_{M1} = \frac{1}{\frac{RePr}{4Nu} + \frac{Nk}{Re.Pr}} \tag{43}$$

$$F_{M2} = \frac{1}{f_D\left(\frac{RePr}{4Nu} + \frac{Nk}{Re.Pr}\right)} \tag{44}$$

Recently Costa *et al.* [109] reconsidered these expressions and proposed a new formulation including the dead volume ratio as defined below:

$$F_{MSC} = \frac{1}{\left(\frac{\Delta P}{Pm}\frac{V_{dr}}{V_e}\frac{\dot{Q}_t}{\dot{Q}_t}\right)} \tag{45}$$

The FOM does not track overall engine efficiency so closely when comparing regenerators of different matrix structures.

The Nasa/Sunpower installation tested several materials as regenerator (see Relevant Websites section). The highest FOM was given by the microfabricated regenerator (**Fig. 34**). According to authors the FOM is the largest and most comprehensive method to judge the regenerator performances.

For a Reynolds number between 10 and 100, the FOM is in the range of 0.07–0.42 for a microfabricated regenerator. The highest value can be rich for Reynolds number about 400.

Gheith *et al.* [110] studied a Gamma type Stirling regenerator (**Fig. 35**) based on FMSC formulation. They proposed a first study to determine the adequate material (aluminum, copper, Monel 400, and stainless steel) and then to determine the adequate porosity (75%, 80%, 85%, 90%, and 95%). The regenerators with 80% and 85% of porosity has, respectively, a FMSC of 0.3 and 0.29. These two matrices present the best porosities of a Gamma Stirling engine regenerator. The FMSC was estimated for the stainless steel matrices of 80% of porosity (**Figs. 36** and **37**).

Different stainless steel regenerators are manufactured with different porosity. The volume ratio increases with porosity due to the increase of its corresponding dead volume. This ratio is a geometrical parameter depending on the volumetric porosity of the regenerator. In our case the expansion space volume (VE) is constant for all experiments. The losses ratio (Q_{loss}/Q_{tot}) decreases initially with porosity until a minimal value for a porosity of 85% the increases with the porosity. The following **Table 12** summarize the effect of some losses.

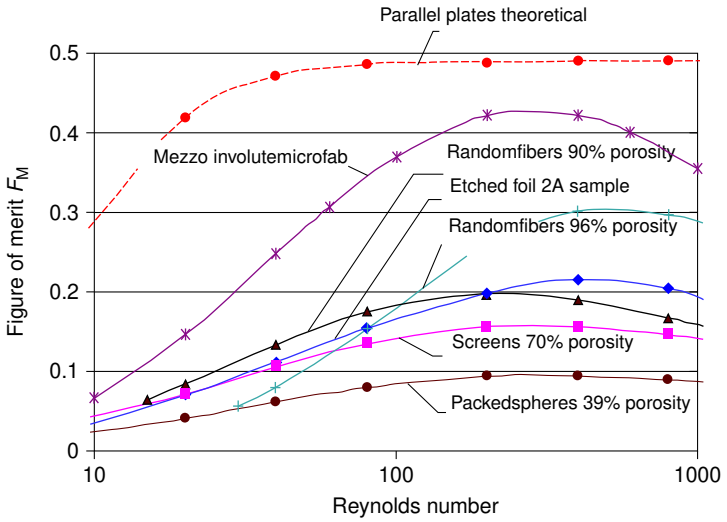

Fig. 34 Figure of merit (FOM) of different regenerator materials, porosities, and Reynolds number. Reproduced from Timoumi Y, Tlili I, Ben Nasrallah S. Performance optimization of Stirling engines. Renew Energy 2008;33:2134–44.

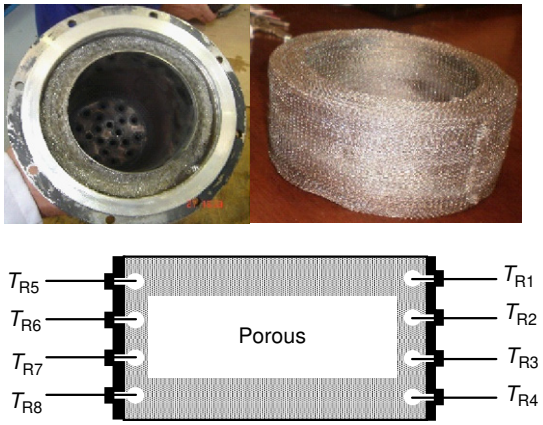

Fig. 35 Gheith *et al*. Stirling regenerators. Reproduced from Gheith R, Aloui F, Ben Nasrallah S. Investigation of regenerator matrix through figure of merit analysis, AJKFluids2015-22087, pp. V001T22A001. doi:10.1115/AJKFluids2015-22087; 2015.

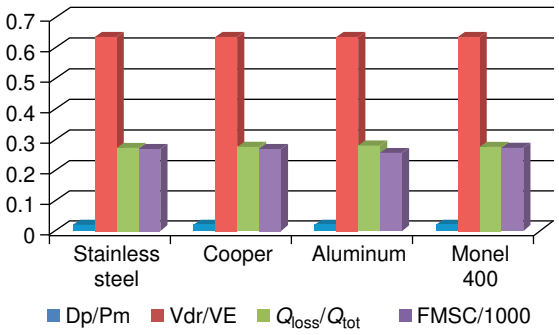

Fig. 36 Figure of merit (FOM) and its different ratios estimated for different regenerator materials. Reproduced from Gheith R, Aloui F, Ben Nasrallah S. Investigation of regenerator matrix through figure of merit analysis, AJKFluids2015-22087, pp. V001T22A001. doi:10.1115/AJKFluids2015-22087; 2015.

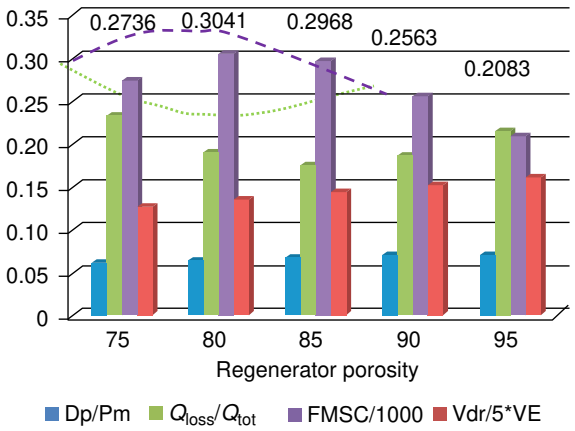

Fig. 37 Figure of merit (FOM) (F_{MSC}) and its constituting ratios estimated for different regenerator porosities: stainless steel material. Reproduced from Gheith R, Aloui F, Ben Nasrallah S. Investigation of regenerator matrix through figure of merit analysis, AJKFluids2015-22087, pp. V001T22A001. doi:10.1115/AJKFluids2015-22087; 2015.

Table 12 Influence of regenerator porosity in thermal losses through regenerator

Parameter	*Porosity < 85%*	*Porosity > 85%*
Thermal losses by external conduction	Low	High
Amount of heat exchanged between the working fluid and the regenerator	Low	High
Heat quantity stored in the regenerator	High	Low
Friction losses	High	Low

Table 13 Effect of operation parameters

Parameters	*Range*	*Influence on asymmetry of temperature between both regenerators' sides*
Cooling flow rates (l/min)	0.26–8.16	Significant effect
Charge pressure (bar)	3–8	Significant effect
Heating temperature (°C)	300–500	The most significant parameter
Operating time (s)	4–20	No effect recorded

4.6.5.2 One-Variate Regenerators Experimentation

The one-variate experimentation was proposed by Gheith *et al.* [3], in order to determine the adequate regenerator for a gamma Stirling engine installation. They found the same result obtained by the FOM formulation [110]. This method needs long time to explore the whole domain of experimentation, a significant experimental time, and does not ultimately represent the complete effect of each parameter on the desired response.

4.6.5.3 Experimental Design Methodology

Experimental design ensures good organization of experimental tests in scientific research or industrial study [111]. This method has several advantages over the one-variant method:

- reduction in the number of test to be carried out to scan the entire field of study;
- possibility to study a large number of factors at the same time;
- detection of single or double interactions between the studied factors;
- modeling of the studied answers;
- optimal precision of the results; and
- optimization of the answers.

Gheith *et al.* [112] applied an experimental design plan to study the effect four operation parameters (**Table 13**) on the asymmetry of temperature between both regenerators' sides.

Based on this study, authors proposed an empirical model for predicting the value of an asymmetry of temperature between both regenerator sides' function of operation parameters.

Table 14 Comparison between experimental methods

	One variate	*Figure of merit (FOM)*	*Experimental design*
Number of tests	• Very important number of tests • Do not scan the entire field of study • Applied to all parameters	Limited	Reduction in the number of test to be carried out Scan the entire field of study Applied for only independent parameters
Results precision	Acceptable precision	Good precision Including losses and Reynolds number	Good precision based on isosurface plot Consider the interaction between studied parameters
Results and perspectives	–	–	Gives an empirical model for predicting results function of studied factors

4.6.5.4 Comparison Between Methods

The presented experimental method to study the Stirling engine presents different advantages and disadvantages, which are summarized in **Table 14**. The choice of the adequate method depends on needed results.

4.6.6 Main Results and Discussion

4.6.6.1 Stirling Engines Performance Investigations

1. Compared to Ericson engine:
   - At nearly the same working conditions, the Stirling engine presents higher global performances (specific indicated work, thermodynamic and exergetic efficiencies) compared with the Ericsson engine [113], due to the presence of a regenerator. The gap between these performances (about 24.18% of global exergetic efficiency and 15.53% of global thermodynamic efficiency) might be reduced using a preheater in the Ericsson engine.
   - According to Hachem *et al.* [113], the proportion of total exergy destruction compared with the exergy flux from the hot source is similar for both engines (respectively 44% and 47% of the exergy flux from the hot source for the Stirling and Ericsson engines). The largest exergy destruction occurs in the compression cylinder, mainly due to generated entropy in the case of the Ericsson engine and due to a similar proportion of generated entropy and of heat loss toward the cold source for the Stirling engine. The regenerator (or preheater for the Ericsson engine) presents an important role to supply the expansion cylinder with a high exergy flux. The exergy recovered reaches about 28% of the destroyed exergy.
2. Effect of operation parameters:
   - The rotation speed is a very determining parameter. The increase of the speed has double effects. On one hand, it favors the exchanges of heat by convection and on the other hand, it increases the losses by viscous friction through the singularities of the thermal machine. Thus, an optimum value of the speed must always be respected to ensure the proper functioning of the Stirling machine [114].
   - The increase of initial charge pressure leads to an increase of working fluid mass, which increases the Stirling engine brake power [14]. However, the load pressure is limited on the one hand by the capacity of the motor to withstand the high pressure (resistance of the materials) and on the other, by the realization of a perfect seal (to reduce the leaks of working gas).
   - The increase of hot end temperature leads to an increase of the thermal exchanged energy. Thus, the increase of Stirling engine brake power. However, the temperature of the hot end should be moderate. It is limited by the melting temperature of the material of the HEX.
3. The efficiency of heater:
   - The exchanged heat and the efficiency in the heater present periodic evolution [115]. All operation parameters (heating temperature, initial filling pressure, and cooling water flow rate) have significant influence. The amount of heat absorbed by the working fluid in the heater increases with the heating temperature, the difference of temperature between both Stirling engine working spaces increases with the cooling water flow rate and the mass for working fluid involved to the process of heat exchange in the heater increases with the initial filling pressure. All this parameters contribute to the amelioration of a Stirling engine heater [115].
4. The CFD modeling:
   - The CFD model gives the trends and the correct values of the influence of the different operating parameters on the performance of the Stirling engine.

4.6.6.2 Stirling Engine Regenerator Investigation

The performance of Stirling engine is closely related to its regenerator's properties. Thus, the regenerator is the most studied compartment of the Stirling engine. The main results are summarized as follows:

1. Thermal losses inside regenerator:
   - The regenerator is the seat of significant losses by internal conduction, by imperfection and pressure drops (caused by friction of working gas with the internal walls of the porous matrix) [14].
   - The maximum losses are recorded in regenerator. According to Ref. [14], it is the set of 44% of viscous loss, 33% of internal conduction loss, and 22% of imperfection loss respectively from the total losses inside it. The Shuttle loss is only recorded in compression and expansion spaces. The mechanical loss is recorded in the engine driving mechanism. They decrease the output brake power of the Stirling engine.
   - These losses depend on the geometrical and physical properties of the regenerator's material [14].
   - The Stirling engine is exposed to continuous internal and external perturbations while operating. However, it cannot change speed quickly [116]. Irreversibilities inside the Stirling engine increase when changing its functioning regime. Thus, thermal losses inside the regenerator increase.
2. Average entropy generation rate in the Stirling engine regenerator:
   - Entropy generation in the regenerator is generated from the irreversibility owing to heat transfer with finite temperature gradients and the friction of fluid flow [117].
   - Entropy generation in the regenerator is associated with a number of parameters including the characteristics of the regenerator (geometry, porosity, and material), the working conditions (temperature ratio between hot and cold source, initial pressure, and rotational engine speed) and the thermophysical properties of the working fluid [117]. Thus, the best regenerator qualities are those corresponding to the minimum entropy generation ($\phi = 0.85$, $L_r/D_r = 1.3$ and stainless steel as matrix material).
   - Compared to air as working fluid, the average entropy generation rate in the regenerator is reduced when using helium as working fluid [117].
   - The average entropy generation rate in the regenerator increases with rotational engine speed, hot end temperature, and initial pressure [117].
3. Regenerators proprieties:
   - The stainless steel material is the most suitable material that can be used as a regenerator. An optimal porosity of 80% can be considered for the porous regenerator. It is recommended to use a high pressure and a low initial filling pressure to maximize regenerator performances [110].
   - The use of copper for air as working fluid must be avoided because of oxidation problem [110].
   - An optimum value of porosity corresponds to the maximum mechanical power [118].
   - According to Ref. [83], thermal losses inside the regenerator are function of regenerator length and diameter (regenerator design). For A 25 W Beta type Stirling prototype, the optimal values for length and diameter are respectively about 60 mm and 22 mm.
4. Optimization methods:
   - The FOM is a rapid tool to evaluate Stirling engine regenerator. To avoid the multiobjective complicated studies the FOM can be used since it considers the major characteristics of porous media regenerators [110].
   - After, the F_{MSC} evaluation tool was calculated for different regenerators having different material (stainless steel, copper, aluminum, Monel) and different porosities (75%, 80%, 85%, 90%, and 95%). The stainless steel and the copper material present the highest F_{MSC} for respectively 0.273 and 0.274.

4.6.7 Future Directions

In order to design and size less polluting and less energy consuming systems, the main goal of the next researches will be the study, using experimental and numerical CFD simulation, the evaluation of an innovate micro-CHP unit that will couple a 1.2-kW double acting Stirling engine to the exhaust gas of an ICE.

In the automotive field, usually the efficiency of current engines does not exceed 40% on their best operating point. In most cases, the yield is well below 20%. A significant part of the losses is in the form of heat evacuated by the cooling circuit and by the exhaust gases. Several technical devices are possible to recover this energy, such as external combustion engines and Stirling engines in particular.

4.6.7.1 Description of the Recovery Process Using the Stirling Engine

In the proposed recovery process, the Stirling engine will be coupled to a generator to power the car's battery and the other car systems consume electrical energy, instead of using electrical power produced directly from the alternator coupled to ICE drive shaft while it is running. It can enhance the amount of power available for the car propulsion. The innovative recovery system will be composed of a gasoline engine and a double acting Stirling engine that is composed of heater, cooler, and motion transmission

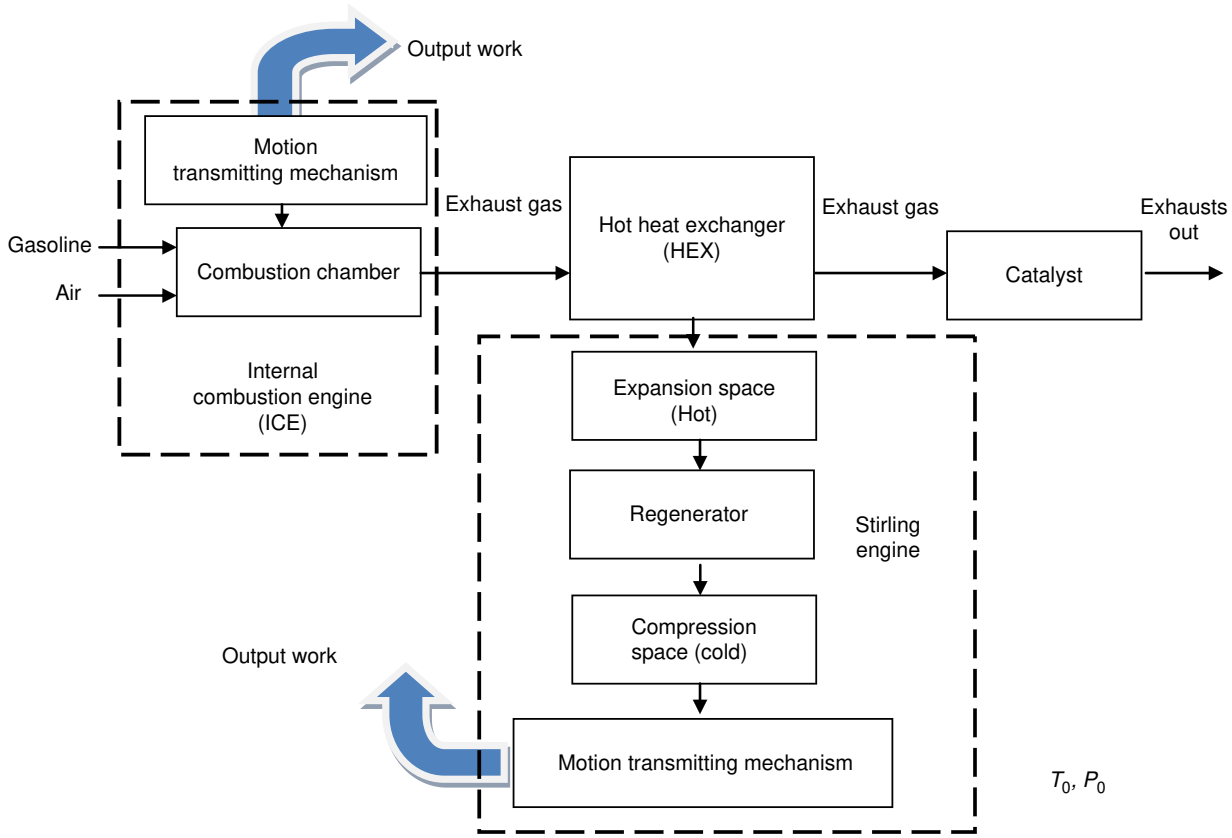

Fig. 38 Equipment of the recovery process.

system coupled to an alternator. The mechanical power produced by the Stirling engine will be used to drive the alternator, thus providing the required electrical power for the different electronic devices inside the car (air conditioning system, electric power steering, electrical windows motors, built-in satellite navigation, etc.). In order to achieve this project, different targets must be accomplished. Fig. 38 presents all these equipments and the main bond between them. The hot exhaust gases from the ICE go through the hot heat exchanger (HEX) in contact with the working gas (helium or nitrogen in this case) in the Stirling engine (SE). On the other side, cold water will go through the cold heat exchanger (CEX) in contact with the working fluid (helium or nitrogen) inside the Stirling engine.

4.6.8 Conclusions

A review of Stirling engine regenerators was proposed in this chapter. The most significant regenerator parameters were presented with their main influences on Stirling engine output and discussed.

The constituting material and the porosity are the most influencing parameters for regenerator performances, which is the main key of the Stirling engine. New material, such as graphite and carbon fiber, can give high thermal efficiency.

The quasi-steady model including thermal losses can give satisfying results compared to experimental ones. The CFD simulations can provide detailed evolution of working fluid particles and help avoiding recirculation zones when designing and sizing new Stirling engine installations.

The FOM is presented as a powerful tool to test several regenerators for the same installation. It provided fast and precise results, with a minimum of experimental investigation measurements series. The experimental design methodology scans the entire field of the study and determine the influence of the interaction between studied factors on the response. This method gives an empirical model (equation) that can link the desired result(s) to the studied factors.

Acknowledgments

This work was supported by the laboratory LAMIH CNRS UMR 8201 (University of Valenciennes), the laboratory LESTE (ENIM, Monastir, Tunisia), the regional Council of Hauts-de-France (province of north of France) and the European Commission within

the International Research Staff Exchange Scheme (IRSES) in the 7th Framework Program FP7/2014-2017/ under REA grant agreement no. 612230. This support is gratefully acknowledged.

In Memory of Our Colleague, Professor Sassi BEN NASRALLAH

This research topic, on the boundary Stirling engine, was initially initiated at the LAMIH laboratory (UMR CNRS 8201) of the University of Valenciennes by Professor Fethi ALOUI and LESTE laboratory of the University of Monastir (Tunisia) and by our colleague, Professor Sassi BEN NASRALLAH, coauthor of this current study, who left us suddenly on June 27, 2017 before the final submission of this paper, after a myocardial heart attack.

We would like firstly to pay a very great tribute to him. Professor Sassi BEN NASRALLAH was an excellent colleague, very serious, scientifically very curious, and very human. With him, we lost more than just a colleague, but a very dear friend and brother.

References

[1] Organ AJ. The air engine: stirling cycle power for a sustainable future. Boca Raton, FL: CRC Press; 2007. ISBN: 978-1-84569-231-5.
[2] Organ AJ. Air engines; 2001. ISBN: 978-1860583385.
[3] Gheith R, Aloui F, Ben Nasrallah S. Study of the regenerator constituting material influence on a gamma type Stirling engine. Mech Sci Technol 2012;26(4):1251–5.
[4] Reader GT, Hooper C. Stirling engines. New York, NY: E & FN Spon; 1983.
[5] Puech P, Tishkova V. Thermodynamic analysis of a Stirling engine including regenerator dead volume. Renew Energy 2011;36:872–8.
[6] Kongtragool B, Wongwises S. Thermodynamic analysis of a Stirling engine including dead volumes of hot space, cold space and regenerator. Renew Energy 2006;31:345–59.
[7] Park SH, Lee YS. An approximate thermal analysis of Stirling engine regenerators. Mech Sci Technol 1993;7(2):113–43.
[8] Andersen SK, Carlsen H, Thomsen PG. Numerical study on optimal Stirling engine regenerator matrix designs taking into account the effects of matrix temperature oscillations. Energy Convers Manag 2006;47:894–908.
[9] Abduljalil AS, Zhibin Y, Jaworski AJ. Selection and experimental evaluation of low-cost porous materials for regenerator applications in thermo-acoustic engines. Mater Des 2011;32:217–28.
[10] Abrahamian RM. On the maximum efficiency of the ideal regenerative stirling cycle. Contemp Phys (Am Acad Sci) 2010;45(3):137–9.
[11] Kongtragool B, Wongwises S. A review of solar powered Stirling engines and low temperature differential Stirling engines. Renew Sustain Energy Rev 2003;7:131–54.
[12] Tanak M, Yamashita F, Chisaka F. Flow and heat transfer characteristics of the Stirling engine regenerator in oscillating flow. JSME 1990;33(2):283–9.
[13] Holman JP. Heat transfer. 9th ed. New York, NY: McGraw-Hill; 2002. ISBN: 0070296391.
[14] Hachem H, Gheith R, Aloui F, Ben Nasrallah S. Global numerical characterization of a γ-Stirling engine considering losses and interaction between functioning parameters. Energy Convers Manag 2015;96:532–43.
[15] Tlili I. Étude et modélisation des Moteurs Stirling, thèse, Ecole Nationale d'Ingénieur de Monastir; 2010.
[16] Alfarawi S, AL-Dadah R, Mahmoud S. Potentiality of new miniature-channels Stirling regenerator. Energy Convers Manag 2017;133:264–74.
[17] Chen WL, Wong KL, Chen HE. An experimental study on the performance of the moving regenerator for a c-type twin power piston Stirling engine. Energy Convers Manag 2014;77:118–28.
[18] Wan B. Stirling engine regenerator. US 20140331689 A1; 2014.
[19] Kato Y, Baba K. Empirical estimation of regenerator efficiency for a low temperature differential Stirling engine. Renew Energy 2014;62:285–92.
[20] Formosa F, Despesse G. Analytical model for Stirling cycle machine design. Energy Convers Manag 2010;51:1855–63.
[21] Gheith R, Aloui F, Ben Nasrallah S. Study of temperature distribution in a Stirling engine regenerator. Energy Convers Manag 2014;88:962–72.
[22] Gheith R, Aloui F, Ben Nasrallah S. Determination of adequate regenerator for a gamma-type Stirling engine. Appl Energy 2015;139:272–80.
[23] Gheith R, Aloui F, Ben Nasrallah S. Optimization of Stirling engine performance based on an experimental design approach. Int J Energy Res 2013;37(12):1519–28.
[24] Wikipedia. Moteur Stirling. Available from: https://fr.wikipedia.org/wiki/Moteur_Stirling.
[25] Organ AJ. Stirling and pulse-tube cryo-coolers: the inside story; 2004. ISBN: 978-1860584619.
[26] Organ AJ. The regenerator and the stirling engine; 1997. ISBN: 978-1860580109.
[27] Walker G, Fauvel R, Gustafson R, van Bentham J. Stirling engine heat pumps. Refrigeration 1982;5(2):91–7.
[28] Martini WR. Stirling engine design manual. Honolulu: University Press of the Pacific; 2004. Reprinted from the 1983 edition. ISBN: 1-4102-1604-7.
[29] Organ AJ. Stirling engine thermodynamic design: without a computer. Cambridge: Regenerative Thermal Machines; 1993. ISBN: 0951808710.
[30] Beale W. Understanding stirling engines. Arlington: VITA; 1984. ISBN: 0-86619-200-X.
[31] Hachem H, Gheith R, Aloui F, Ben Nasrallah S, Dincer I. Exergy assessment of heat transfer inside a beta type Stirling engine. Exergy 2016;20(2):186–202.
[32] Kaushik SC, Tyagi SK, Bose SK, Singhal MK. Performance evaluation of irreversible Stirling and Ericsson heat pump cycles. Therm Sci 2002;41(2):193–200.
[33] Ross A. Stirling cycle engines. Phoenix; 1981.
[34] Ross A. Making Stirling engines; 2nd ed. Solar Engines; 1993.
[35] Urieli I, Berchowitz D. Stirling cycle engine analysis. Bristol: Institute of Physics Publishing; 1984. ISBN: 0-85274-435-8.
[36] Dincer I, Rosen MA. Exergy: energy, environment and sustainable development. Amsterdam: Elsevier; 2007.
[37] Lanzetta F, Boucher J, Nika P. Etude et réalisation d'une pompe à eau Fluidyne, Journée SFT du 8 décembre: Machines thermiques exotiques, Institut FEMTO-ST, CNRS UMR 6174, Département CREST Parc technologique, Belfort; 2004.
[38] Boucher J, Lanzetta F, Nika P. Optimization of a dual free piston Stirling engine. Appl Therm Eng 2007;27:802–11.
[39] Cheng C-H, Yang H-S. Theoretical model for predicting thermodynamic behavior of thermal-lag Stirling engine. Energy 2013;49:218–28.
[40] Cheng C-H, Yang H-S, Jhou B-Y, Chen Y-C, Wang Y-J. Dynamic simulation of thermal-lag Stirling engines. Appl Energy 2013;108:466–76.
[41] Gheith R, Aloui F, Tazerout M, Ben Nasrallah S. Experimental investigations of a gamma Stirling engine. Energy Res 2012;36:1175–82.
[42] Tlili I, Musmar SA. Thermodynamic evaluation of a second order simulation for Yoke Ross Stirling engine. Energy Convers Manag 2013;68:149–60.
[43] Thombare DG, Verma SK. Technological development in the Stirling cycle engines. Renew Sustain Energy Rev 2008;12:1–38.
[44] Meijer RJ. The Philips hot gas engine with rhombic drive mechanism. Philips Tech Rev 1958;2(9):245–76. [chapter 2].
[45] Walker G, Senft JR. Free piston stirling engines. Berlin: Springer-Verlag; 1985. ISBN:3-540-15495-7.
[46] Descombes G, Magnet JL. Moteur non conventionnels. Techniques de l'ingénieur, BM 2 593; 1997. p. 1–34.
[47] West C. Liquid piston stirling engines. New York, NY: Van Nostrand Reinhold; 1983. ISBN: 0-442-29237-6.

[48] Bakos GC, Antoniades C. Techno-economic appraisal of a dish/stirling solar power plant in Greece based on an innovative solar concentrator formed by elastic film. Renew Energy 2013;60:446–53.
[49] Hafez AZ, Soliman A, El-Metwally KA, Ismail IM. Solar parabolic dish Stirling engine system design, simulation, and thermal analysis. Energy Convers Manag 2016;126:60–75.
[50] Sadrameli SM. Mathematical models for the simulation of thermal regenerators: a state-of-the-art. Renew Sustain Energy Rev 2016;58:462–76.
[51] Clean Enegy. Gasbox 901 data sheet. Available from: http://www.stirlingengines.org.uk/manufact/manf/misc/whi.html.
[52] INFINEA. 30-kw maintenance-free solar dish engine. DOE solar programs annual review, Austin, TX, April 22, 2008; 2008.
[53] Nepveu F, Ferriere A, Bataille F. Thermal model of a dish/Stirling systems. Sol Energy 2009;83(1):81–9.
[54] Whisper Tech Ltd. Whispergen. Product specifications.
[55] Crema L, Alberti F, Bertaso A, Bozzolo A,, *et al*. Development of a pellet boiler with Stirling engine for m-CHP domestic application. Energy, Sustain Soc 2011;1:5.
[56] Walker G. Stirling engines. Oxford: Oxford University Press; 1980. ISBN: 0-19-856209-8.
[57] Graham TR, Hooper C. Stirling engines. London: E. & F. N. Spon; 1983. ISBN 0-419-12400-4.
[58] West C. Principles and applications of Stirling engines. New York, NY: Van Nostrand; 1986. ISBN0-442-29273-2.
[59] Tlili I, Timoumi Y, Ben Nasrallah S. Analysis and design consideration of mean temperature differential Stirling engine for solar application. Renew Energy 2008;33:1911–21.
[60] Obernberger I, Carlsen H, Biedermann F. State-of-the art and future developments regarding small-scale biomass CHP systems with a special focus on ORC and Stirling engine technologies. In: International Nordic bioenergy conference; 2003.
[61] De Paepe M, D'Herdt P, Mertens D. Micro-CHP systems for residential applications. Energy Convers Manag 2006;47:3435–46.
[62] Cacabelos A, Eguía P, LuísMíguez J, Rey G, Elena Arce M. Development of an improved dynamic model of a Stirling engine and a performance analysis of a cogeneration plant. Appl Therm Eng 2014;73:608–21.
[63] Thiers S, Aoun B, Peuportier B. Experimental characterization, modeling and simulation of a wood pellet micro-combined heat and power unit used as a heat source for a residential building. Energy Build 2010;42(6):896–903.
[64] Conroy G, Duffy A, Ayompe L. Validated dynamic energy model for a Stirling engine m-CHP unit using field trial data from a domestic dwelling. Energy Build 2013;62:18–26.
[65] Finkelstein T, Polonski C. Development and testing of a Stirling cycle machine with characteristics suitable for domestic refrigerators: Report W/M (3A).U.5, English Electric Company Ltd., Whetstone; 1959.
[66] Le'an S, Yuanyang Z, Liansheng L, Pengcheng S. Performance of a prototype Stirling domestic refrigerator. Appl Therm Eng 2009;29:210–5.
[67] Ataer OE, Karabulut H. Thermodynamic analysis of the V-type Stirling-cycle refrigerator. Int J Refrig 2005;28:183–9.
[68] Giannetti N, Milazzo A. Thermodynamic analysis of regenerated air-cycle refrigeration in high and low pressure configuration. Int J Refrig 2014;40:97–110.
[69] Otaka T, Ota M, Murakami K. Study of performance characteristics of a small stirling refrigerator. Heat Transf Asian Res 2002;31(5):344–61.
[70] Formosa F, Badel A, Lottin J. Equivalent electrical network model approach applied to a double acting low temperature differential Stirling engine. Energy Convers and Manag 2014;78:753–64.
[71] Hofacker M, Kong K, Barth EJ. A lumped-parameter dynamic model of a thermal regeerator for free-piston Stirling engines. In: 2009 ASME dynamic systems and control conference & Bath/ASME symposium on fluid power and motion control. DSCC2009-2741, October 12–14, 2009, Hollywood, CA; 2009. p. 1–8.
[72] Timoumi Y, Tlili I, Ben Nasrallah S. Performance optimization of Stirling engines. Renew Energy 2008;33:2134–44.
[73] Costa SC, Barrutia H, Esnaola JA, Tutar M. Numerical study of the pressure drop phenomena in wound woven wire matrix of a stirling regenerator. Energy Convers Manag 2013;67:57–65.
[74] Chen WL, Wong KL, Po LW. A numerical analysis on the performance of a pressurized twin power piston gamma-type Stirling engine. Energy Convers Manag 2012;62:84–92.
[75] Clearman WM, Cha JS, Ghiaasiaan SM, Kirkconnell CS. Anisotropic steady-flow hydrodynamic parameters of microporous media applied to pulse tube and Stirling cryocooler regenerators. Cryogenics 2008;48:112–21.
[76] Tao YB, Liu YW, Gao F, Chen XY, He YL. Numerical analysis on pressure drop and heat transfer performance of mesh regenerators used in cryocoolers. Cryogenics 2009;49:497–503.
[77] Eid E. Performance of a beta-configuration heat engine having a regenerative displacer. Renew Energy 2009;34:2404–13.
[78] Andersen SK, Carlsen H, Thomsen PG. Numerical study on optimal Stirling engine regenerator matrix designs taking into account the effects of matrix temperature oscillations. Energy Convers Manag 2006;47:894–908.
[79] Tlili I, Timoumi Y, Ben Nasrallah S. Analyse and design consideration of mean temperature differential Stirling engine for solar application. Renew Energy 2008;33:1911–21.
[80] Xiao G, Peng H, Fan H, Sultan U, Ni M. Characteristics of steady and oscillating flows through regenerator. Heat Mass Transf 2017;108:309–21.
[81] Dietrich M, Yang LW, Thummes G. High-power Stirling-type pulse tube cryocooler: observation and reduction of regenerator temperature in homogeneities. Cryogenics 2007;47:306–14.
[82] Cheng C-H, Yu Y-J. Dynamic simulation of a beta-type Stirling engine with cam-drive mechanism via the combination of the thermodynamic and dynamic models. Renew Energy 2011;36:714–25.
[83] Hachem H, Gheith R, Aloui F, Ben Nasrallah S. Optimization of an air-filled beta type Stirling refrigerator. Refrigeration 2017;76:296–312.
[84] Glushenkov M, Sprenkeler M, Kronberg A, Kirillov V. Single-piston alternative to Stirling engines. Appl Energy 2012;97:743–8.
[85] Ahmadi MH, Hosseinzade H, Sayyaadi H, Mohammadi AH, Kimiaghalam F. Application of the multi-objective optimization method for designing a powered Stirling heat engine: design with maximized power, thermal efficiency and minimized pressure loss. Renew Energy 2013;60:313–22.
[86] Ahmadi MH, Mohammadi AH, Dehghani S, Barranco-Jiménez MA. Multi-objective thermodynamic-based optimization of output power of solar dish-stirling engine by implementing an evolutionary algorithm. Energy Convers Manag 2013;75:438–45.
[87] Ahmadi MH, Sayyaadi H, Dehghani S, Hosseinzade H. Designing a solar powered Stirling heat engine based on multiple criteria: maximized thermal efficiency and power. Energy Convers Manag 2013;75:282–91.
[88] Luo Z, Sultan U, Ni M, Peng H, Shi B, Xiao G. Multi-objective optimization for GPU3 Stirling engine by combining multi-objective algorithms. Renew Energy 2016;94:114–25.
[89] Zahi N, Boughamoura A, Dhahri H, Ben Nasrallah S. Flow and heat transfer in a cylinder with a porous medium insert along the compression stroke. Porous Media 2008;11(6).
[90] Kozeny J. Flow in porous media. S.B. Akad. Wiss Abt IIa 126 (2);1927.
[91] Ergun S. Fluid flow through packed columns. Chem Eng Prog 1952;48(2):89–94.
[92] Stouffs P. Dimensionnement Optimal des Volumes de Compression et de Détente des Moteurs Stirling. In: To be presented at the french thermal congress SFT, vol. 8; 2000. p. 851–6.
[93] MacDonald IF, El-Sayed MS, Mow K, Dullien FAL. Flow through porous media- the Ergun equation revisited. Ind Eng Chem Fundam 1979;18:199–208.
[94] Hicks RE. Pressure drops in packed beds of spheres. Ind Eng Fundam 1970;9:500–2.
[95] Rose HE, Rizk AMA. Further researches in fluidflow through beds of granular materials. Proc Instit Mech Eng 1970;160:493–503.
[96] Tallmadge JA. Packed bed pressure drop – an extension to high Reynolds numbers. AIChE J 1970;16:1092–3.

[97] Lee JS, Ogawa K. Pressure drop through packed beds. Chem Eng 1974;27:691–3.
[98] Walker G. Stirling cycle machines. Oxford: Clarendon Press; 1973.
[99] Senft JR. An introduction to low temperature differential stirling engines. River Falls, WI: Moriya Press; 1996. ISBN: 0-9652455-1-9.
[100] Reader GT, Hooper C. Stirling engines. London; New York, NY: E. & F.N. Spon; 1983.
[101] Zhigang L, Yoshihiko H, Yohei K, Dawei T. Analysis of a high performance model Stirling engine with compact porous-sheets heat exchangers. Energy 2014;64:31–43.
[102] Salazar JL, Chen W-L. A computational fluid dynamics study on the heat transfer characteristics of the working cycle of a β-type Stirling engine. Energy Convers Manag 2014;88:177–88.
[103] Chen W-L, Yang Y-C, Salazar JL. A CFD parametric study on the performance of a low-temperature differential γ-type Stirling engine. Energy Convers Manag 2015;106:635–43.
[104] Costa S-C, Tutar M, Barreno I, *et al.* Experimental and numerical flow investigation of Stirling engine regenerator. Energy 2014;72:800–12.
[105] Ibrahim MB, Tew RC. Stirling convertor regenerators. Boca Raton, FL: CRC Press; 2012. ISBN: 978-1-43983006-2.
[106] Gedeon D. Regenerator figures of merit, (CSU Microfab Figures of Merit.tex), Unpublished memorandum to Microfabrication Team; 2003.
[107] Gedeon D Digression on regenerator figure of merit calculations, (CSU Microfab FMerit Consistency.tex), Unpublished memorandum to Microfabrication Team; 2003.
[108] Gedeon D, Wood G. Oscillating-flow regenerator test rig: woven screen and metal felt results. NASA-CR-190689, NAS 1.26:190689; 2012.
[109] Costa SC, Barreno I, Tutar M, Esnaola JA. Figure of merit analysis of a stirling engine regenerator matrix through experimental studies. ISEC: Bilbao, Spain; 2014.
[110] Gheith R, Aloui F, Ben Nasrallah S. Investigation of regenerator matrix through figure of merit analysis. In: ASME/JSME/KSME 2015 joint fluids engineering conference; 2015. doi:10.1115/AJKFluids2015-22087.
[111] Goupy J. Introduction aux plans d'expériences. Paris: Dunod; 2001.
[112] Gheith R, Aloui F, Ben Nasrallah S. Optimization of a Stirling engine performances: a study based on experiments design approach. In: ASME 2012 fluids engineering division summer meeting collocated with the ASME 2012 Heat transfer summer conference and the ASME 2012 10th International Conference on Nanochannels, Microchannels, and minichannels, vol. 1: symposia, Parts A and B; 2012. p. 1085–90. doi:10.1115/FEDSM2012-72239.
[113] Hachem H, Creyx M, Gheith R, *et al.* Comparison based on exergetic analyses of two hot air engines: a gamma type stirling engine and an open joule cycle ericsson engine. Entropy 2015;17(11):7331–48.
[114] Hachem H, Gheith R, Aloui F, Dincer I, Ben Nasrallah S. Energetic and exergetic performance evaluations of an experimental beta type stirling machine. Progress in Clean Energy: Novel Systems and Applications, vol. 2. New York, NY: Springer; 2015. p. 735–53. ISBN: 978-3-319-17030-5. doi:10.1007/978-3-319-17031-2.
[115] Gheith R, Hachem H, Aloui F, Ben Nasrallah S. Experimental and theoretical investigation of Stirling engine heater: parametrical optimization. Energy Convers Manag 2015;105:285–93.
[116] Hachem H, Gheith R, Aloui F, Ben Nasrallah S. Experimental study of the operation conditions of stability on a gamma Stirling engine. In: ASME 2016 fluids engineering division summer meeting collocated with the ASME 2016 heat transfer summer conference and the ASME 2016 14th international conference on nanochannels, microchannels, and minichannels; 2016. doi:10.1115/FEDSM2016-7912.
[117] Hachem H, Gheith R, Ben Nasrallah S, Aloui F. Entropy generation for oscillatory flow inside thermal-lag type Stirling engine: numerical analysis. In: ASME 2017 fluids engineering division summer meeting; volume 1A, symposia: keynotes; advances in numerical modeling for turbomachinery flow optimization; fluid machinery; industrial and environmental applications of fluid mechanics; pumping machinery; 2017; doi:10.1115/FEDSM2017-69010.
[118] Gheith R, Aloui F, Tazerout M, Ben Nasrallah S. Study of the regenerator porosity influence on gamma type Stirling engine performances. In: ASME-JSME-KSME 2011 Joint Fluids Engineering Conference; volume 1, symposia – parts A, B, C, and D; 2011. p. 3573–8. doi:10.1115/AJK2011-17013.
[119] Darcy H. Les Fontaines Publiques de la ville de Dijon. Dalmont: Paris; 1856.

Further Reading

NASA. A microfabricated segmented-involute-foil regenerator for enhancing reliability and performance of Stirling engines Phase II Final Report for the radioisotope power conversion technology NRA Contract NAS3-03124, NASA/CR-215006; 2007.

Relevant Websites

https://www.stirlingengine.com/
American Striling Company.
http://www.boehm-stirling.com/en/engines.html
Boehm.
http://cleanergy.com/
CleanEregy.
http://diystirlingengine.com/stirling-engine-generator/
DIY Stirling Engine.
http://www.microgen-engine.com/
Microgen.
https://www.grc.nasa.gov/www/tmsb/stirling.html
NASA.
https://www.ohio.edu/mechanical/stirling/intro.html
Ohio education: Background and Introduction.
http://www.robertstirlingengine.com/
Stirling engine.
https://en.wikipedia.org/wiki/Stirling_engine
Stirling engine.
http://sunpowerinc.com/1kw-stirling-engine/
Sunpower.